

UNIVERSITÉ DU QUÉBEC

**ÉTUDE DE LA CIRCULATION DANS
LE BASSIN DE FOXE (CANADA)**

RAPPORT PRÉSENTÉ À L'UNIVERSITÉ DU QUÉBEC À RIMOUSKI

comme exigence partielle du programme

de doctorat en océanographie

PAR

MARC DEFOSSEZ

Décembre 2008

UNIVERSITÉ DU QUÉBEC À RIMOUSKI
Service de la bibliothèque

Avertissement

La diffusion de ce mémoire ou de cette thèse se fait dans le respect des droits de son auteur, qui a signé le formulaire « *Autorisation de reproduire et de diffuser un rapport, un mémoire ou une thèse* ». En signant ce formulaire, l'auteur concède à l'Université du Québec à Rimouski une licence non exclusive d'utilisation et de publication de la totalité ou d'une partie importante de son travail de recherche pour des fins pédagogiques et non commerciales. Plus précisément, l'auteur autorise l'Université du Québec à Rimouski à reproduire, diffuser, prêter, distribuer ou vendre des copies de son travail de recherche à des fins non commerciales sur quelque support que ce soit, y compris l'Internet. Cette licence et cette autorisation n'entraînent pas une renonciation de la part de l'auteur à ses droits moraux ni à ses droits de propriété intellectuelle. Sauf entente contraire, l'auteur conserve la liberté de diffuser et de commercialiser ou non ce travail dont il possède un exemplaire.

REMERCIEMENTS ET AVANT-PROPOS

Cette thèse a été réalisée, jusqu'à son décès, sous la direction de Monsieur François Saucier, professeur à l'Institut des sciences de la mer de Rimouski (ISMER). La codirection a été assurée par Messieurs Paul Myers, professeur associé à l'Université d'Alberta et président de la Société canadienne de météorologie et d'océanographie, et Daniel Caya, professeur associé à l'Université du Québec à Montréal et directeur de l'équipe de simulations numériques au Consortium OURANOS-UQAM. Le comité de thèse était composé des personnes précédemment citées et de Monsieur Jean-François Dumais, professeur et directeur des programmes à l'ISMER. La soutenance a eu lieu le 6 octobre 2008 à l'ISMER devant le jury d'évaluation composé de:

Monsieur Éric Hudier (président du jury), professeur à l'Université du Québec à Rimouski;

Madame Daniela Di Iorio (examinatrice externe), professeur associée à l'Université de Georgia, Athens, USA;

Monsieur Jean-François Dumais (examineur interne), professeur à l'Institut des sciences de la mer de Rimouski;

Monsieur Paul Myers (codirecteur de thèse), professeur associé à l'Université d'Alberta;

Monsieur Daniel Caya (codirecteur de thèse), professeur associé à l'Université du Québec à Montréal.

Je remercie ici toutes les personnes qui ont contribué à la réalisation de ce travail, en particulier les membres du comité de thèse ainsi que Monsieur Hudier et Madame Di Iorio pour leurs précieux commentaires qui ont permis d'améliorer le rapport final.

RÉSUMÉ

Le bassin de Foxe est une région mal connue du système de la baie d'Hudson, un ensemble formé de trois mers intérieures à l'extrême nord du Canada, car il est recouvert de glace plus de six mois par an et que cela le rend difficile d'accès. Il est susceptible d'être très affecté par les changements climatiques, car son océanographie dépend fortement de la formation, de la couverture et du déplacement de la glace de mer. La présente étude se propose donc d'éclaircir certains aspects de la circulation dans le bassin, en particulier la circulation des eaux profondes dans le chenal de Foxe et la circulation hivernale. Elle s'appuie pour cela sur un ensemble d'observations nouvelles issues de mouillages pluriannuels, de 2003 à 2006, complétées par des simulations réalisées sur la période 2001-2005 à l'aide d'un modèle couplé glace de mer-océan avec forçages atmosphériques. Ces données ont permis de mettre en évidence la propagation au fond du chenal d'un courant de gravité qui prend son origine dans les polynies côtières à chaleur latente de l'ouest du bassin de Foxe. Ces eaux denses renouvellent chaque année plus des deux tiers des eaux profondes dans le chenal et ont assez d'énergie pour franchir un seuil à 180 m de profondeur et déborder dans la baie d'Hudson. Le volume des eaux denses produites dans les polynies a pu être estimé en calculant les flux de chaleur à l'interface mer-atmosphère et a été trouvé égal à $1,53 \cdot 10^{12} \text{ m}^3$. L'ouverture des polynies en plein hiver entraîne la synchronisation des écoulements d'eau dense, sous forme de cascade et de convection profonde. Ce phénomène est dépendant des conditions atmosphériques, donc de l'oscillation arctique, et devrait répondre au réchauffement global. L'hiver et l'été peuvent être définis par le taux de croissance de la glace de mer sur le bassin. La glace induit des changements sur la circulation générale et les marées, y compris à 150 m de profondeur. Cette glace possède aussi une dynamique très active et les courants qu'elle forme sont réguliers et forts, de l'ordre de 25 cm s^{-1} . Même si elle pénètre parfois dans le nord-est de la baie d'Hudson, elle n'y reste pas et finit par rejoindre la Mer du Labrador via le détroit d'Hudson, sous forme solide ou fondue; le calcul indique qu'un tiers de toute la glace produite dans le bassin de Foxe est ainsi exportée. Enfin, le bilan des transferts d'eau de mer et de sel au travers d'une section en sortie du bassin montre que la circulation estuarienne de ce dernier forme un couple positif-négatif, la partie positive étant cependant perturbée par le passage du courant de gravité.

TABLE DES MATIÈRES

REMERCIEMENTS ET AVANT-PROPOS	i
RÉSUMÉ	ii
TABLE DES MATIÈRES	iii
LISTE DES TABLEAUX	vii
LISTE DES FIGURES	viii
LISTE DES ABBRÉVIATIONS, SIGLES ET ACRONYMES	xi
NOMENCLATURE	xiv
I. INTRODUCTION GENERALE	1
II. MULTI-YEAR OBSERVATIONS OF DEEP WATER RENEWAL IN FOXE BASIN, CANADA	10
ABSTRACT	11
II.1. INTRODUCTION	12
II.2. OBSERVATIONS AND METHOD	16
II.2.1. Oceanographic data	16
II.2.2. Data processing	17
II.3. DENSE WATER SPEED IN FOXE CHANNEL	28
II.3.1. Vertical propagation speed of the dense water signal	28
II.3.2. Calculation of horizontal mean speed of the dense water current	29
II.4. DISCUSSION	31

II.4.1. Origin of the dense water mass detected at depth in Foxe Channel	31
II.4.2. Recurrence of the dense water pulse at the bottom of Foxe Channel	37
II.4.3. Effect of the dense water circulation on the water column in Foxe Channel	40
II.5. CONCLUSION	43
III. ANALYSIS OF A DENSE WATER PULSE FOLLOWING MID-WINTER OPENING OF POLYNYAS IN WESTERN FOXE BASIN, CANADA	45
ABSTRACT	46
III.1. INTRODUCTION	47
III.2. DATA DESCRIPTION AND METHOD	52
III.2.1. Oceanographic and meteorological data	52
III.2.2. Satellite data	56
III.3. RESULTS	61
III.3.1. Heat fluxes calculations in western Foxe Basin's polynyas	61
III.3.1.1. Calculation for the 2003-2004 winter	61
III.3.1.2. Calculation for the years 1984-2006	65
III.3.2. Production of dense water in western Foxe Basin's polynyas	69
III.3.2.1. Calculation of the produced sea-ice and rejected salt masses	69
III.3.2.2. Calculation of the dense water volume	73
III.4. DISCUSSION	77
III.4.1. Dense water production in western Foxe Basin's polynyas	77
III.4.2. Consequences of the mid-winter opening of western Foxe Basin's polynyas	79

III.4.3. Atmospheric pressure and synoptic scale	81
III.5. CONCLUSION	88
IV. COMPARING WINTER AND SUMMER ESTUARINE CIRCULATION IN FOXE BASIN, CANADA	90
ABSTRACT	91
IV.1. INTRODUCTION	92
IV.2. MODEL DESCRIPTION AND OBSERVATIONS	98
IV.2.1. Model	98
IV.2.2. Observations	100
IV.3. FOXE BASIN PHYSICAL OCEANOGRAPHY	102
IV.3.1. Winter and summer definition	102
IV.3.2. Sea-ice dynamics	102
IV.3.3. Water characteristics and mean circulation	109
IV.3.3.1. In winter	110
IV.3.3.1.1. At the surface	110
IV.3.3.1.2. At the bottom	113
IV.3.3.2. In summer	114
IV.3.3.2.1. At the surface	114
IV.3.3.2.2. At the bottom	115
IV.4. MASS TRANSFERT BETWEEN THE SURROUNDING PARTS OF FOXE BASIN	117
IV.4.1. Seawater and salt transport	117

IV.4.2 Ice transport	121
IV.5. TIDAL ANALYSIS	125
IV.6. DISCUSSION AND CONCLUSION	128
V. CONCLUSION GENERALE	131
BIBLIOGRAPHIE	xviii

LISTE DES TABLEAUX

Tableau II.1	Characteristics of the T-S mixing lines at the bottom of Foxe Channel during the dense water pulse for the years 2004 and 2005	25
Tableau III.1	Main topographic elements of Foxe Basin	50
Tableau III.2	Main characteristics of western Foxe Basin's polynyas	60
Tableau III.3	Relative contribution of the sensible H_S^* and latent H_L^* heats, and of the upwards $H_{LW\ up}^*$ and downwards $H_{LW\ down}^*$ longwaves to the net heat exchanged at the polynyas' surface	66
Tableau III.4	Calculation of sea-ice mass (M_{ice}), rejected salt mass (M_{salt}) and dense water volume (V_{dw}) produced in western Foxe Basin's polynyas during the 2003-2004 winter	70
Tableau IV.1	Mean speed and total distance covered by the Lagrangian tracers leaving Foxe Basin	108
Tableau IV.2	Velocity and phase components vs. tidal constituents in Foxe Channel	126

LISTE DES FIGURES

Figure II.1	Foxe Basin and surrounding parts of the Hudson Bay system based on ETOPO2	13
Figure II.2	Deep water seasonal cycle observed in 2004-2006 in Foxe Channel	18
Figure II.3	Temperature over the last 200 m of the water column in Foxe Channel	20
Figure II.4	Temporal profile of the dense water mass flowing in Foxe Channel	22
Figure II.5	Vertical propagation of the dense water signal	23
Figure II.6	Comparison between the salinity at 360 and 150 m depth in Foxe Channel	26
Figure II.7	T-S diagram representing the mixing of Foxe Channel's deep waters with the incoming dense waters for 2004 and 2005	27
Figure II.8	Dense water circulation and cascade in Foxe Basin	34
Figure II.9	Satellite image showing the sea-ice distribution on March 4, 2004, over western Foxe Basin	36
Figure III.1	Hudson Bay system and Foxe Basin	48
Figure III.2	Foxe Channel's deep water response to sea surface atmospheric events	53
Figure III.3	Atmospheric parameters averaged from 1984 to 2006 at Repulse Bay and Hall Beach weather stations	57

Figure III.4	Satellite images showing the opening of polynyas in western Foxe Basin	58
Figure III.5	Net daily integrated sea-atmosphere heat exchanges in western Foxe Basin's polynyas	64
Figure III.6	Sea-atmosphere heat exchanges averaged from 1984 to 2006 in Lyon Inlet's polynya, in the polynya along Melville Peninsula's eastern coast, and in Hall Beach's polynya	68
Figure III.7	Schematic representation of frazil ice and dense water formation following intense heat loss at a latent heat polynya's surface.....	74
Figure III.8	Comparison of surface air pressure in the north and south of the Hudson Bay system	84
Figure III.9	Consequence of the meridional inversion of the atmospheric pressure in mid-winter and over the Hudson Bay system on the wind velocity field at 10 m in Foxe Basin	85
Figure III.10	Schematic representation of the incoming dense water mass at the bottom of Foxe Channel in winter and of its effects on sedimentation	86
Figure IV.1	Hudson Bay system and Foxe Basin	93
Figure IV.2	Simulated ice growth rate averaged over Foxe Basin	103
Figure IV.3	Simulted ice growth rate averaged over the winter in Foxe Basin ..	105
Figure IV.4	Simulated sea-ice trajectory in Foxe Basin	107
Figure IV.5	Simulated temperature, salinity and seawater velocity fields, averaged over winter and summer in Foxe Basin	111
Figure IV.6	Vertical simulate seawater (a) and salt transport (b) through the cross section defined in Foxe Channel	118

Figure IV.7	Simulated sea-ice thickness averaged over the winter in Foxe Basin	122
Figure IV.8	Satellite image taken on June 20, 2002 over Foxe Basin and its surrounding parts	123
Figure V.1	Comparaison entre les observations et les simulations en température et en salinité au fond du chenal de Foxe	132

LISTE DES ABBRÉVIATIONS, SIGLES ET ACRONYMES

AO	Arctic Oscillation
BB	Baffin Bay
CAA	Canadian Arctic Archipelago
CI	Coats Island
CLIVAR	Climate Variability
CTD	Conductivity Temperature Depth
DS	Davis Strait
ESA	European Space Agency
ETOPO2	Earth Topography 2 minutes
FB	Foxe Basin
FC	Foxe Channel
FDD	Freezing Degree Days
FHS	Fury and Hecla Strait
FP	Foxe Peninsula
GB	Gulf of Boothia
HaB	Hall Beach
HB	Hudson Bay
HS	Hudson Strait
K1	constituent luni-solaire déclinatoire diurne de la marée

LI	Lyon Inlet
LS	Labrador Sea
M2	constituent lunaire semi-diurne de la marée
MERICA	Mers Intérieures du Canada
MI	Mansel Islands
MP	Melville Peninsula
N2	constituent lunaire elliptique semi-diurne de la marée
NA	North Atlantic
NI	Nottingham Island
NOAA	National Oceanic and Atmospheric Administration
O1	constituent lunaire déclinatoire diurne de la marée
P _{1,2}	Points sur la droite de mélange avant et après le début du courant de gravité
PCI	Prince Charles Island
P _{MI,2}	Points sur la droite de mélange avant et après la fin du courant de gravité
RB	Repulse Bay
RWS	Roes Welcome Sound
S2	constituent solaire semi-diurne de la marée
SBS	Sea Bottom Salinity
SBT	Sea Bottom Temperature
SD	Standard Deviation
SI	Southampton Island
SSS	Sea Surface Salinity

SST	Sea Surface Temperature
Sv	Sverdrup (unité: $1\text{ Sv} \equiv 10^6 \text{ m}^3\text{s}^{-1}$)
T-S	Temperature-Salinity
T ₁₋₁₀	numéros des Traceurs
UNESCO	United Nations Educational, Scientific and Cultural Organization
UTC	Coordinated Universal Time
WI	Winter Island

NOMENCLATURE

e	épaisseur de la glace de mer
f	paramètre de Coriolis
g	accélération de la gravité
n	nombre d'années
s	pente topographique
u	composante ouest-est du vecteur courant
v	composante sud-nord du vecteur courant
v_{dw}	vitesse de la masse d'eau dense
w	composante fond-surface du vecteur courant
z	profondeur
A	surface d'une polynie
A_{cs}	surface d'une section transverse du chenal de Foxe comprise entre le fond et le sommet de la masse d'eau dense
A_{max}	surface maximale d'une polynie active
C_{E10}	coefficient de transfert en volume pour la chaleur latente
C_{H10}	coefficient de transfert en volume pour la chaleur sensible
C_p	chaleur spécifique de l'air à pression constante
H_L	flux de chaleur latente

H_{LW}	flux des ondes longues
H_{LWdown}	flux des ondes longues dirigées vers le bas
H_{LWup}	flux des ondes longues dirigées vers le haut
H_{net}	flux de chaleur net
H_S	flux de chaleur sensible
L	chaleur latente de fusion de l'eau de mer
L_v	chaleur latente de vaporisation de l'eau de mer
M_{ice}	masse de la glace de mer
M_{salt}	masse de sel rejeté dans la colonne d'eau
Q_{10}	densité de vapeur atmosphérique
Q_s	densité de vapeur à la surface de la mer
Q_{salt}	débit de sel par une section
Q_{wat}	débit d'eau par une section
S	salinité de l'eau de mer
S_{dw}	salinité des eaux denses
S_i	salinité moyenne de la glace de mer
S_{mean}	salinité moyenne dans le bassin de Foxe
S_s	salinité moyenne de surface
S_{sect}	salinité sur la section
S_{sw}	salinité des eaux environnantes
T	température de l'eau de mer
T_{10}	température de l'air à 10 m

T_{dw}	température des eaux denses
T_s	température de l'eau de surface dans une polynie
T_{sw}	température des eaux environnantes
$U_{//}$	composante longitudinale du courant dans le chenal de Foxe
U_{\perp}	composante transversale du courant dans le chenal de Foxe
V_{dw}	volume des eaux denses produites
V_{dw0}	volume initial des eaux denses
V_{sw}	volume des eaux environnantes servant à produire les eaux denses
W_{10}	composante nord-ouest sud-est de la vitesse du vent à 10 m
ε_{air}	émissivité de l'air
ε_{sea}	émissivité de la surface de la mer
θ	déphasage de la composante M2 de la marée
ρ	densité de l'eau de mer
ρ_0	densité de l'eau douce
ρ_{air}	densité de l'air
ρ_{dw}	densité des eaux denses
ρ_{ice}	densité de la glace de mer
ρ_{sw}	densité des eaux environnantes
σ	constante de Stefan-Boltzmann
τ	temps caractéristique de résidence des eaux profondes

- $\Phi_{//}$ phase de la composante longitudinale du courant dans le chenal de Foxe
- Φ_{\perp} phase de la composante transversale du courant dans le chenal de Foxe

I. INTRODUCTION GENERALE

La géographie particulière du bassin de Foxe en fait un sujet très intéressant pour l'étude de la circulation dans une mer arctique-subarctique, car le bassin ne comporte qu'un plateau au nord et un chenal au sud et qu'il est bien isolé des mers voisines par des complexes formés d'îles et de seuils. Ceci donne une topographie relativement simple et qui facilite le suivi des masses d'eau entrantes, sortantes ou s'écoulant à l'intérieur du bassin. Mais c'est cette même géographie qui est responsable du déficit en données dans la région, car l'éloignement et le climat rigoureux compliquent les campagnes de mesure, surtout en hiver quand la glace de mer rend la navigation impossible. Ainsi, des pans entiers de l'océanographie physique du bassin de Foxe étaient jusqu'à présent négligés, en particulier la circulation des eaux profondes dans le chenal de Foxe et la circulation hivernale. Le but principal de cette thèse est donc d'apporter des réponses sur ces aspects méconnus du bassin de Foxe, mais c'est aussi de dresser un état des lieux sur sa situation actuelle afin de fournir une base pour évaluer l'impact des changements climatiques à venir.

Avant d'aborder le cœur du problème, il convient de préciser quelques éléments géographiques sur le bassin de Foxe. Le bassin est la partie la plus septentrionale du système de la baie d'Hudson, un ensemble composé de trois grandes mers intérieures, et il subit à la fois les influences de l'Arctique et du continent nord américain. Son centre est assez bien défini par le point de coordonnées 66°N et 80°O , c'est à dire que le bassin est

traversé en son milieu par le cercle polaire arctique, ce qui a une grande incidence sur la formation des glaces à cause des flux radiatifs solaires faibles sur cette région en hiver. Ses moitiés nord et sud se distinguent surtout par la bathymétrie: la partie nord est formée à l'est par des estrans et à l'ouest par un chenal peu profond, variant d'environ 15 à 150 m et longeant sur 300 km la côte est de la péninsule de Melville, tandis que la partie sud est essentiellement formée du chenal de Foxe, long de 350 km et atteignant des profondeurs de l'ordre de 450 m. Le bassin est compris entre l'île de Baffin au nord et à l'est, l'île Southampton au sud et la péninsule de Melville à l'ouest. Il communique avec l'Arctique via le détroit de Fury et Hecla, avec la mer du Labrador via le détroit d'Hudson, et avec la baie d'Hudson via le détroit de Roes Welcome et le passage entre les îles Southampton et Nottingham. La surface du bassin est approximativement de $0,2 \cdot 10^{12} \text{ m}^2$, pour un volume de $0,2 \cdot 10^{14} \text{ m}^3$. Comparativement, la baie d'Hudson fait $0,8 \cdot 10^{12} \text{ m}^2$ en surface et $1,1 \cdot 10^{14} \text{ m}^3$ en volume, et le détroit d'Hudson $0,2 \cdot 10^{12} \text{ m}^2$ et $0,4 \cdot 10^{14} \text{ m}^3$. Le bassin de Foxe est donc relativement "petit" vis-à-vis de ses voisins. Cependant, c'est aussi une voie par laquelle transitent une fraction des eaux arctiques qui se rendent dans l'Atlantique Nord, augmentées au passage par l'apport fluvial et glaciaire. Le bassin joue donc un rôle important dans la circulation thermohaline et cela justifie, dans le contexte des changements climatiques, le regain d'intérêt que cette région suscite depuis quelques années.

L'aspect le moins bien connu de la circulation dans le bassin de Foxe est certainement la circulation des eaux profondes dans le chenal de Foxe. En effet, il aura fallu attendre l'année 2003 pour que des mouillages y soient déployés dans le cadre des missions

pluriannuelles MERICA (Saucier *et al.*, 2004b). Les séries temporelles obtenues permettent désormais de suivre sans interruption l'évolution saisonnière des propriétés des eaux profondes dans le chenal. Auparavant, il n'existait que des mesures sur quelques stations, réalisées lors de campagnes océanographiques estivales. Les données de ces campagnes, assez anciennes et rares de surcroît, n'ont pas permis de fournir une description précise de la circulation profonde, même si la présence d'eau très froide ($< -1,80$ °C) et salée ($> 33,75$) dans le chenal de Foxe a été attestée dès 1955 par Campbell (1964), et de nouveau en 1982 par Jones et Anderson (1994). Comme ces auteurs ne disposaient que d'observations éparses, tant spatialement que temporellement, ils n'ont pu que conjecturer sur la formation et la circulation de ces eaux denses, sans jamais pouvoir valider leurs scénarios. Ces lacunes dans la connaissance de l'océanographie du bassin de Foxe en ont engendré d'autres. Par exemple, des mesures en alcalinité et en carbonates ont montré qu'une partie des eaux profondes du chenal de Foxe déborde dans la baie d'Hudson (Jones et Anderson, 1994), mais il n'a pas été alors possible de quantifier ce phénomène.

Le premier objectif de cette thèse est donc d'améliorer la compréhension de la circulation profonde dans le chenal de Foxe. L'accent est mis principalement sur le renouvellement des eaux profondes afin d'en estimer l'ampleur ainsi que la variabilité interannuelle. Cette question est importante, non seulement parce qu'elle permet de mieux décrire la circulation dans le bassin de Foxe, mais aussi parce qu'elle conditionne la ventilation en oxygène et donc la biologie au fond du chenal. La recherche de l'origine des eaux profondes ainsi que les conséquences de leur circulation sur la colonne d'eau sont

incluses dans cet objectif.

La méthode employée pour réaliser cette première étude repose principalement sur les observations en température et en salinité issues des mouillages MERICA 2003 à 2006 acquises du bas de la colonne d'eau (150 m) jusqu'au fond du chenal (360 ou 440 m, selon le mouillage). Ces trois années successives de données permettent d'étudier la récurrence et la variabilité des phénomènes saisonniers. Des données simulées issues du modèle numérique développé par Saucier *et al.* (2004a) sont aussi utilisées pour rechercher l'origine des eaux denses du bassin de Foxe à l'aide de traceurs lagrangiens, selon une procédure de pistage à rebours.

Une des particularités des mers polaires est que ce sont des régions qui produisent des quantités importantes d'eau froide riche en saumure lors du gel des eaux salées de surface. Ainsi, dans l'Arctique, elles contribuent à la maintenance de la couche supérieure de l'halocline, ce qui a des conséquences sur la circulation thermohaline dans l'Atlantique Nord. Aagaard *et al.* (1981) ont estimé que l'ensemble des plateaux arctiques produisaient environ 2,5 Sv ($1 \text{ Sv} \equiv 10^6 \text{ m}^3\text{s}^{-1}$) d'eau dense; quant à Cavalieri et Martin (1994), ils ont calculé que la contribution des polynies côtières arctiques était comprise entre 0,7 et 1,2 Sv. Dans le cas du bassin de Foxe, les résultats du premier objectif montrent (voir chapitre II) que les eaux denses détectées au fond du chenal de Foxe se forment dans les polynies côtières à chaleur latente de l'ouest du bassin, et qu'elles se propagent ensuite comme un courant de gravité dans le chenal. Le problème qui se pose alors naturellement est de

vérifier que, d'une part, la production d'eau dense dans les polynies suffit à expliquer le renouvellement des eaux profondes et que, d'autre part, la chronologie des différents évènements est compatible avec ce scénario.

Le second objectif complète donc le premier en fournissant une analyse quantitative des mécanismes menant à la propagation le long du chenal de Foxe de la masse d'eau dense trouvant son origine dans les polynies de l'ouest du bassin de Foxe. Ceci revient essentiellement à calculer les flux de chaleur entre la surface de la mer et l'atmosphère au niveau des polynies puis à en déduire les quantités de glace et d'eau dense produites. L'intérêt de ce type d'analyse ne fait aucun doute, car les paramètres de ces calculs dépendent fortement des conditions météorologiques présentes en hiver au dessus du bassin et il est donc probable que les changements climatiques tels qu'anticipés par les modèles numériques (Johns *et al.*, 1997; Emori *et al.*, 1999) affecteront sensiblement les résultats actuels. Ce deuxième objectif est complété par une discussion sur le lien probable entre l'intensité de la production d'eau dense dans les polynies et l'index de l'oscillation arctique, ce qui permet d'étendre la portée de cette recherche au-delà du seul cadre du bassin de Foxe.

Les calculs des flux de chaleur pour cette seconde étude nécessitent la connaissance de la dynamique spatiale des polynies qui est déterminée ici à l'aide d'images satellites montrant leur ouverture au milieu de l'hiver. Ils nécessitent aussi la connaissance des vents et de la température de l'air qui sont obtenus à partir des enregistrements de deux stations

météorologiques situées au nord-ouest du bassin de Foxe (à Hall Beach) et au sud-ouest (à Repulse Bay). Ces mesures proviennent des bases de données d'Environnement Canada, elles ont été acquises toutes les heures à l'altitude de 10 m; dans cette thèse, elles ont en plus été extrapolées à midi chaque jour (cette extrapolation a été rendue nécessaire à cause des données manquantes). Les calculs de flux sont réalisés pour l'hiver 2003-2004, car, dans le bassin, cette année peut être considérée comme standard du point de vue météorologique. De plus, ces calculs sont généralisés à l'aide d'une quasi-climatologie sur 21 ans consistant à moyenniser les données, à partir du 1er janvier de chaque année, et couvrant la période 1984-2006.

Les premier et second objectifs définis aux paragraphes précédents se concentrent principalement sur le renouvellement des eaux profondes du bassin de Foxe. Bien que cela soit indispensable pour comprendre la circulation dans le bassin, et même si cela peut donner des informations sur les débordements d'eau dense du bassin vers la baie d'Hudson, cela ne suffit pas à décrire la circulation générale ni les échanges avec les mers voisines. Il est donc nécessaire de compléter cette thèse avec une description des courants et de la répartition en température et salinité à l'échelle du bassin de Foxe dans son ensemble. Des travaux antérieurs (Prinsenbergh, 1986; Saucier *et al.*, 2004a) ont signalé que la circulation dans le bassin était estuarienne, c'est à dire gouvernée par les gradients de densité entre les masses d'eau douce jouxtant les masses d'eau salée. Mais ces travaux restent assez vagues en ce qui concerne le type de circulation estuarienne, bien que Prinsenbergh (1986) ait mentionné, sans vraiment le développer, que le bassin pouvait être vu comme un large

estuaire négatif en hiver et positif en été. De plus, ces travaux se contentent généralement d'indiquer que les courants sont affaiblis et que parfois leur sens s'inverse en hiver. Pourtant, l'action de la couverture de glace ne se limite pas à réduire les échanges de chaleur à l'interface mer-atmosphère ni à ajouter de la friction et de l'amortissement à l'interface mer-glace: elle retire aussi des quantités non négligeables d'eau douce à la surface de la mer lorsqu'elle se forme. Or, ce dernier point est loin d'être anecdotique, car, ainsi que l'ont montré El-Sabh *et al.* (1997), les zones côtières des mers polaires sont susceptibles de connaître une circulation estuarienne négative quand l'extraction d'eau douce en surface par formation de glace excède l'apport dû au ruissellement. Ce phénomène peut modifier profondément les flux de matière et mérite d'être étudié de manière approfondie. De plus, MacDonald (2000) a aussi introduit la notion de couple positif-négatif pour les estuaires à haute latitude, en insistant sur la sensibilité de ces couples aux variations climatiques.

Le troisième objectif de cette thèse est donc double: d'une part fournir une description aussi précise que possible de la circulation générale dans le bassin de Foxe, ce qui inclut la circulation de la glace de mer, et d'autre part caractériser le type de circulation estuarienne du bassin afin de voir si elle forme un couple positif-négatif. Une étude à profondeur moyenne (150 m) dans le chenal de Foxe est aussi fournie pour déterminer l'influence du couvert de glace sur les courants de marée; l'étude en surface ayant déjà été réalisée par Saucier *et al.* (2004a).

La description et la caractérisation de la circulation dans le bassin de Foxe reposent entièrement sur le modèle numérique développé et décrit en détail par Saucier *et al.* (2004a). Ce modèle baroclinique donne des résultats très réalistes dans les mers côtières peu profondes et reproduit particulièrement bien les phénomènes à mésoéchelle. C'est donc un très bon outil pour cette troisième étude, car les simulations permettent d'obtenir des données en température, en salinité, en courant et sur les caractéristiques (épaisseur, taux de croissance-fonte, vitesse) de la glace de mer en tout point du bassin et à tout instant sur la période 2001 à 2005. Il faut noter que bien que le pas de temps interne du modèle soit de cinq minutes, les sorties sont moyennées ici sur trois heures pour limiter la taille des fichiers résultats. Ceci est amplement suffisant pour obtenir une bonne précision dans les calculs puisque cette période inclut les principaux constituants de la marée qui est essentiellement de type semi-diurne dans le bassin. En considérant que le passage entre la pointe est de l'île Southampton et la pointe ouest de la péninsule de Foxe sépare le bassin de Foxe à la fois de la baie d'Hudson et du détroit d'Hudson, ce qui revient à "court-circuiter" l'île Nottingham, il n'existe alors que trois voies d'accès au bassin: par les détroits de Fury et Hecla et de Roes Welcome, et par le passage décrit ci-dessus. Les deux premières voies représentent des entrées du bassin, c'est à dire que le transport d'eau en moyenne annuelle se fait vers le bassin, donc la troisième est nécessairement une sortie. C'est pourquoi c'est au niveau de cette dernière qu'est définie la section sur laquelle sont effectués les calculs de transfert de masse d'eau. L'analyse harmonique des marées à mi-profondeur dans le chenal de Foxe est réalisée non pas avec des données simulées, qui sont bien adaptées aux calculs de moyennes sur des portions de la grille numérique, mais plutôt avec des mesures en

courant issues de la campagne MERICA 2005, car ces observations permettent d'obtenir une meilleure précision en un point unique.

Le premier objectif est développé dans le Chapitre II qui a fait l'objet d'un article scientifique publié en 2008 dans la revue *Atmosphere-Ocean*, sous le titre: "*Multi-year observations of deep water renewal in Foxe Basin, Canada*". Le second objectif est développé dans le Chapitre III; il fait lui aussi l'objet d'un article qui a été accepté avec corrections mineures dans la revue *Dynamics of Atmospheres and Oceans*, sous le titre: "*Analysis of a dense water pulse following mid-winter opening of polynyas in western Foxe Basin, Canada*". Quant au troisième objectif, il est développé dans le Chapitre IV qui est également écrit sous la forme d'un article; il est prévu qu'il soit soumis à une revue spécialisée en modélisation océanographique physique sous le titre: "*Comparing winter and summer estuarine circulation in Foxe Basin, Canada*". Toutes les revues dans lesquelles ces articles sont ou seront publiés sont internationales et à comité de lecture. La conclusion générale de cette thèse est donnée dans le Chapitre V qui résume les principaux thèmes abordés ainsi que les résultats obtenus.

**II. MULTI-YEAR OBSERVATIONS OF DEEP WATER
RENEWAL IN FOXE BASIN, CANADA**

ABSTRACT

New oceanographic mooring data recorded between 2004 and 2006 show each year an abrupt arrival of cold and saline water at the bottom of Foxe Channel. Foxe Channel is the deepest part of Foxe Basin, an arctic/subarctic inland sea in the Hudson Bay system. This dense water mass is detected at depth in the middle of the channel at the beginning of spring. It is characterized by a sharp temperature drop and salinity rise. This pulse-like phenomenon is recurrent, although there is some interannual variability depending on the severity of the preceding winter. The dense water probably originates from western Foxe Basin's coastal polynyas. A gravity current in Foxe Channel flows southeastwards and significantly modifies the water column along the channel by raising the isotherms by 140 m. The water column responds to the dense water pulse with a time lag of one month. Although the pulse lasts only three months, it renews more than $2/3^{\text{rd}}$ of the deep waters in Foxe Channel and is therefore an important component of Foxe Basin general circulation. This shows that the pulse is an energetic event and that the newly advected dense waters may have enough kinetic energy to overflow the sill between Foxe Basin and Hudson Bay.

II.1. INTRODUCTION

Foxe Basin (FB) is an inland sea included in the Hudson Bay (HB) system, Canada (Fig. II.1). The basin is well delimited from the other regions of the system either by sills or constrictions that control and limit deep water circulation. FB may be divided into four parts, the three largest are: a) a wide and less than 50 m deep shelf starting from the tip of Foxe Peninsula (FP) and covering the eastern and northern parts of the basin; b) a shallow, widening and gently sloped channel reaching 100 m depth along Melville Peninsula (MP) in the western part; and c) Foxe Channel (FC), a channel 400 km long and 100 km wide reaching depths of 450 m. The fourth, smaller and off-center part of FB is called Repulse Bay (RB) which is a depression reaching 200 m depth, located in southwest FB where it connects to HB via Roes Welcome Sound (RWS).

Arctic water coming from the Gulf of Boothia (GB) enters FB through Fury and Hecla Strait (FHS) where it is well mixed by currents and tides (Sadler, 1982; Godin and Candela, 1987); the estimated transport is 0.04 Sv ($1 \text{ Sv} = 10^6 \text{ m}^3 \text{ s}^{-1}$) in winter (Sadler, 1982) and 0.1 Sv in summer (Barber, 1965). This arctic water is less dense than the waters of FB and tends to flow at the surface (Prinsenberg, 1986). FB is an important contributor to the general circulation in the HB system: in summer, freshwater due to runoff and ice melting is exported by surface currents from FB to the other parts of the HB system while denser water enters the basin underneath and, in winter, some of FB's deep waters overflow into HB while surface water reenters the basin (Prinsenberg, 1986;

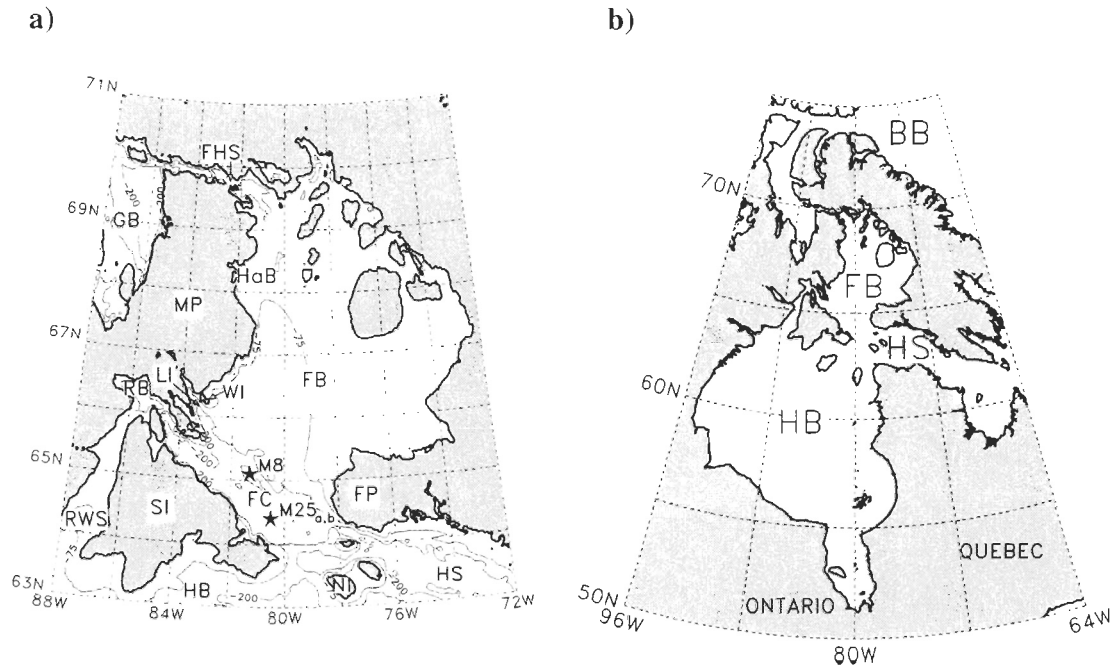


Fig. II.1. Foxe Basin (a) and surrounding parts (b) of the Hudson Bay system based on ETOPO2 (Earth Topography 2-minutes, NOAA). The locations of the moorings are shown with black stars. BB stands for Baffin Bay, FB for Foxe Basin, FC for Foxe Channel, FHS for Fury and Hecla Strait, FP for Foxe Peninsula, GB for Gulf of Boothia, HaB for Hall Beach, HB for Hudson Bay, HS for Hudson Strait, LI for Lyon Inlet, MP for Melville Peninsula, NI for Nottingham Island, RB for Repulse Bay, RWS for Roes Welcome Sound, SI for Southampton Island, and WI for Winter Island.

Jones and Anderson, 1994; Ingram and Prinsenber, 1998; Saucier *et al.*, 2004a). However, the particulars of this circulation are poorly known, especially the dense water component, because FB is a remote region subject to severe climatic conditions. The eight-month long nearly complete sea-ice cover over the basin explains the lack of wintertime data.

Until 2003, there were no year-long time series of measurable physical quantities in FB except in the northwestern corner of the basin for the year 1955-1956 (Grainger, 1959). The few available data come mainly from oceanographic surveys made in 1955 and 1956 (Campbell, 1964) and in 1982 (Jones and Anderson, 1994; Tan and Strain, 1996). Therefore, publications about FB are scarce; Prinsenber (1986) gives the most comprehensive review to date of FB's physical oceanographic aspects.

In 1955 and to a lesser extent in 1956, Campbell (1964) found a cold and saline water mass at depth in FC. This occurrence is described as a cascade of dense water by Ivanov *et al.* (2004). Saucier *et al.* (2004a), with the help of a numerical model, reports also the renewal of deep waters at depth over 300 m in FC. These findings, however, are not supported by year-long observations in temperature and salinity which are needed to characterize this dense water mass and its associated currents.

The goal of this paper is to investigate the deep water renewal and interannual variability at the bottom of FB. It uses new data coming from three oceanographic moorings deployed from 2003 to 2006 at depth in FC. The details of the moorings and data are given in Section II.2. In these observations and for the first time, the abrupt arrival of a dense water mass has been detected each year in the channel. The main characteristics of this pulse-like phenomenon are described in Section II.3. Its origin, its recurrent nature and

its consequences on the deep water renewal and over the water column in FC are discussed in Section II.4. The conclusion of this paper is given in Section II.5.

II.2. OBSERVATIONS AND METHOD

II.2.1. Oceanographic data

The oceanographic data used in this study come from three moorings that were deployed through the program MERICA (*MERs Intérieures du Canada*, Saucier *et al.*, 2004b), northern component, funded by the Department of Fisheries and Oceans, Canada. This research program started in 2003; it involves the long term monitoring of the climate variability and biological productivity of the HB system.

The first mooring consisted of a CTD (Conductivity Temperature Depth, SBE-19 from Sea-Bird Electronics) deployed at the bottom of FC from August 2003 to August 2004 at 440 m depth. Its position indicated by M8 in Fig. II.1a was 65.14 °N and 81.34 °W, which corresponds to FC's deepest trough. The sampling rate of salinity, temperature and depth was set to 15 minutes. The precision and resolution of the sensors are, respectively, 10^{-3} Sm^{-1} and 10^{-4} Sm^{-1} in conductivity, $10^{-2} \text{ }^{\circ}\text{C}$ and $10^{-3} \text{ }^{\circ}\text{C}$ in temperature, and 1.0 dbar and 0.1 dbar in pressure.

The second and third moorings (M25_{a,b} in Fig. II.1a) were equipped with the same CTD model (Sea-Bird SBE-19) than at M8. M25_a was deployed from August 2004 to August 2005 and M25_b from September 2005 to September 2006. They were both moored at 360 m depth at the bottom of FC and their position was 64.37 °N and 80.55 °W. The sampling rate of M25_{a,b}'s CTD sensors was set to 30 minutes with the same sensors' precision and resolution than at M8.

Additionally, Mooring M25_a had temperature sensors (Minilog12: VEMCO-AMIRIX Systems Inc.) distributed from the depth of 357 to 155 m. These devices have a precision of 0.1 °C with a resolution of 0.015 °C, and their sampling rate was set to one hour. This paper also uses the salinity data sampled every hour by the conductivity sensor of a current meter (S4 from InterOcean Systems Inc.) deployed at 150 m depth at M25_a. The nominal precision and resolution in conductivity of InterOcean's S4 are $2 \cdot 10^{-4} \text{ Sm}^{-1}$ and 10^{-4} Sm^{-1} , respectively.

II.2.2. Data processing

In Fig. II.2, the temperature and salinity time series from moorings M8 and M25_{a,b} are plotted on the same graph in order to show the continuity from one year to another of the properties of deep water masses in FC. It is important to note that M8 and M25_{a,b} are 93 km apart and that they are almost aligned with FC. The vertical dashed line in Fig. II.2 marks the gap between the moorings. This configuration has proved itself useful when following the dense water signal flowing along the channel. In Fig. II.2a, the freezing point curve has been calculated according to the depth of each mooring using Millero and Leung's formula (1976). When the freezing point is computed at the surface instead of the mooring's depth, it matches well with the portion of the temperature curve corresponding to the passing of the cold water mass ($T \leq -1.8 \text{ °C}$) for the years 2004 and 2005. This strongly suggests that the freezing waters found at depth in FC are the result of ice formation at the sea surface and that the produced waters keep their characteristics after they sink.

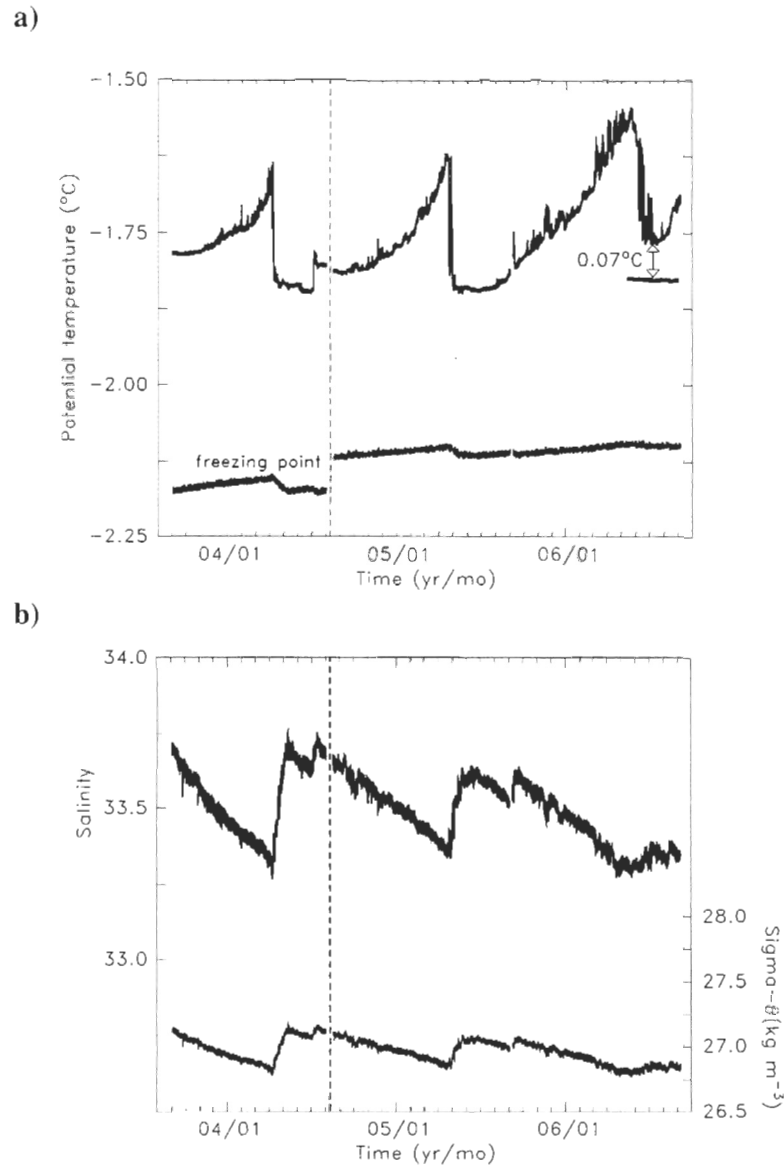


Fig. II.2. Deep water seasonal cycle observed in 2004-2006 in Foxe Channel. Moorings M8 (2004) and M25 (2005 and 2006) data are separated by the dashed line. The thick (thin) lines on **a** and **b** represent the temperature (freezing point) and the salinity ($\text{sigma-}t$) time series, respectively. On **a**, the double arrow shows the gap for the year 2006 between the fragment of curve of the freezing point calculated at the sea surface and the cold waters during the pulse. The break in the freezing point curve on **a** is due to the 80 m difference of depth between M8 and M25.

In 2006, the match between the temperature curve and the freezing point at the surface is less obvious since there is a gap of 0.07 °C. Only the part from June to August 2006 of the freezing point at the surface is drawn in Fig. II.2a for comparison with the temperature curve. Since the 2006 dense waters are likely produced by a similar freezing process than in 2004 and 2005, the gap is probably due to some additional mixing with the surrounding waters. In Fig. 2b, the UNESCO (1981, 1983) algorithms for the sea water density and potential temperature have been used to calculate the sigma- θ curve. The high frequency component of the recorded signal being weak compared to the main seasonal signal, it was not deemed necessary to filter the data in Fig. II.2 to remove tidal effects.

In Fig. II.3, the temperature data from 155 m to the bottom of FC have been low-pass filtered by a fourth order Butterworth filter with a cutoff period equal to 25 hours. This filtering is needed because the original time series, especially the data above 300 m depth, are more affected by the tides as the depth decreases; in other words, the filtering of the time series below 300 m depth does not effectively alter the original data. Note that this same filter is used throughout the paper for the other data. In Fig. II.3a, the interval in depth between each time series is equal to 12 m except for the last two sensors (165 and 155 m) which are 10 m apart. In order to ensure that all curves are on the same baseline, the first 25 hours of each time series have been averaged and the result displayed above each curve at the initial time (September 14, 2004). Fig. II.3b corresponds to three vertical temperature profiles taken just before (average from April 19 to 20, 2005), during (average from April 23 to 24, 2005) and after (average from May 25 to 26, 2005) the pulse-like arrival of dense

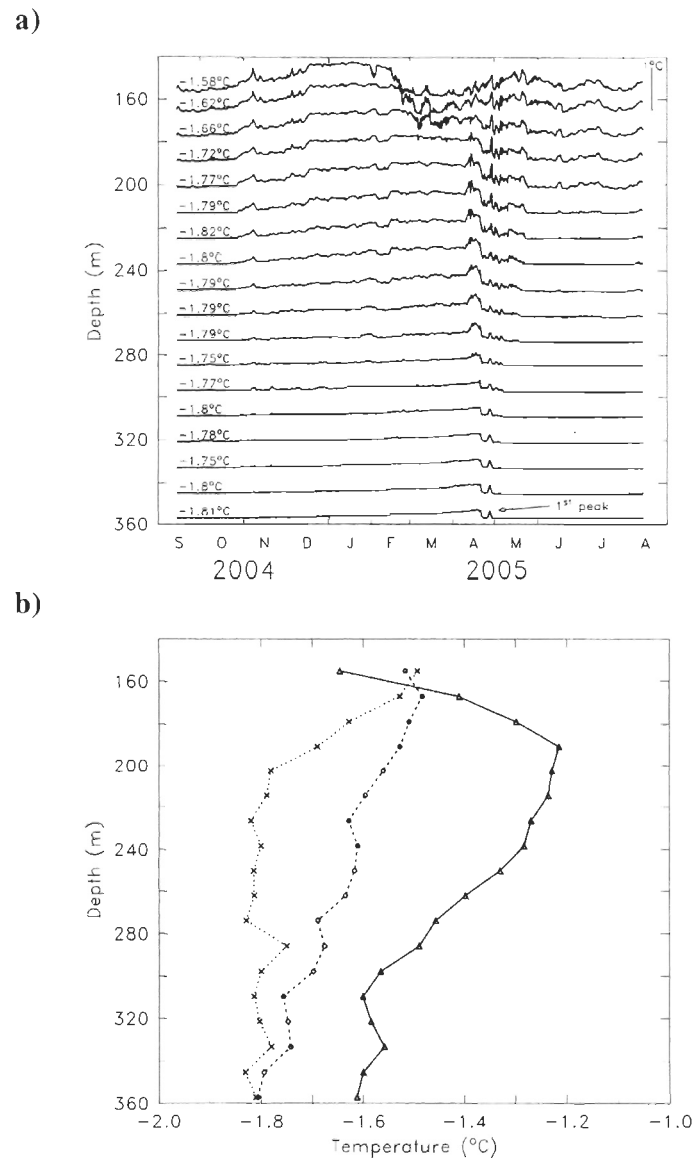


Fig. II.3. Temperature over the last 200 m of the water column in Foxe Channel. All data are low-pass filtered. The temperature at the start of each times series on **a** gives the baseline while the scale is shown in the upper right of the figure. The arrow on **a** indicates the first peak used to estimate the vertical propagation time and speed. The profiles in temperature on **b** are drawn for the periods averaged between April 19-20 (triangles, plain line), April 23-24 (circles, dashed line) and May 25-26 (X, dotted line) for the year 2005.

water in the channel.

From the data in Fig. II.3a, it is possible to reconstruct the time evolving profile of the dense water front at the bottom of FC. This is shown in Fig. II.4 by using a mask discriminating all temperatures above $-1.8\text{ }^{\circ}\text{C}$. The dashed line represents a second order polynomial fit to visualize the profile, so that $depth = -0.038\text{ day}^2 - 2.391\text{ day} + 362.742$ and $357\text{ m} \leq depth \leq 225\text{ m}$. Note that if the speed of the front is considered approximately constant, then multiplying the time coordinates of Fig. II.4's data by this speed would give the actual spatial shape of the front. Also, Fig. II.4 suggests that the wedge formed by the new dense waters has a height of 140 m. This height is greater than the difference in depth between the moorings M8 and M25_{a, b} ($440 - 360 = 80\text{ m}$) and legitimates the presentation of temperature and salinity time series on the same graph (Fig. II.2), since M8 and M25_{a, b} see the same deep water masses.

Fig. II.3a's time series are also useful to estimate the vertical propagation time and speed of the dense water signal, which are shown in Fig. II.5. In particular, the small peak seen just after the temperature drop in Fig. II.3a, which is probably due to the adjustment of the water column caused by the passing of the dense water mass, can be used for each time series because its pattern is easy to identify. For example, this peak occurs on April 28, 2005 at 01 h UTC (Coordinated Universal Time) for the time series at 357 m depth and on April 29, 2005 at 15 h UTC for the one at 155 m. The reference time used for Fig. II.5a corresponds to the peak detected at 357 m depth while, in Fig. II.5b, the vertical propagation speed is calculated from the temperature sensor at the depth of 321 m in order to take into account the thickness of the dense water front.

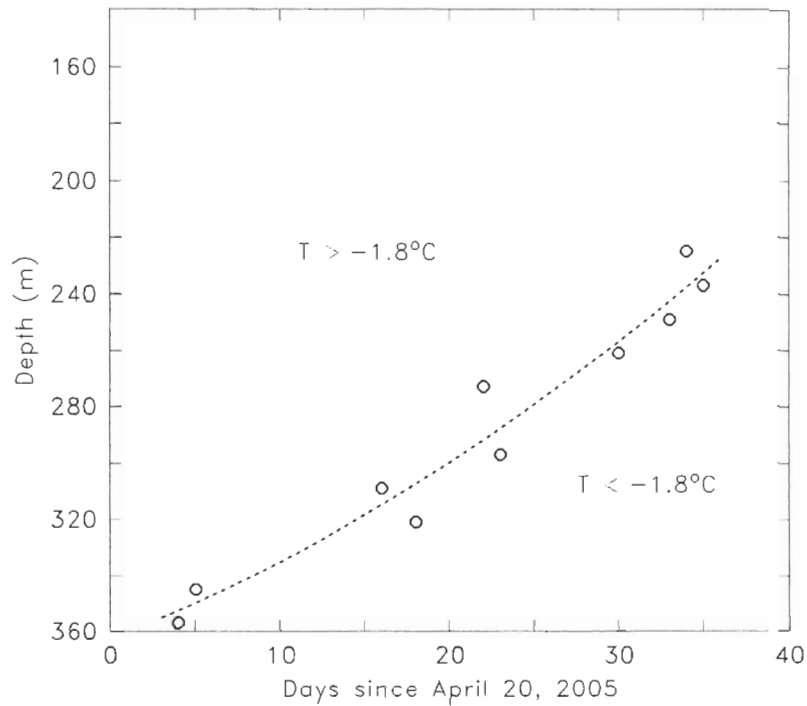


Fig. II.4. Temporal profile of the dense water mass flowing in Foxe Channel. The detection at the bottom of the channel of this water mass gives the reference time ($t_0 = 0$ day) of the plot. For a given depth, the point corresponds to the number of days after t_0 from the time the temperature falls below -1.8°C . The dashed line is a second order polynomial fit of the points; it separates the old deep waters ($T > -1.8^\circ\text{C}$, left of the line) from the new advancing dense waters ($T < -1.8^\circ\text{C}$, right of the line).

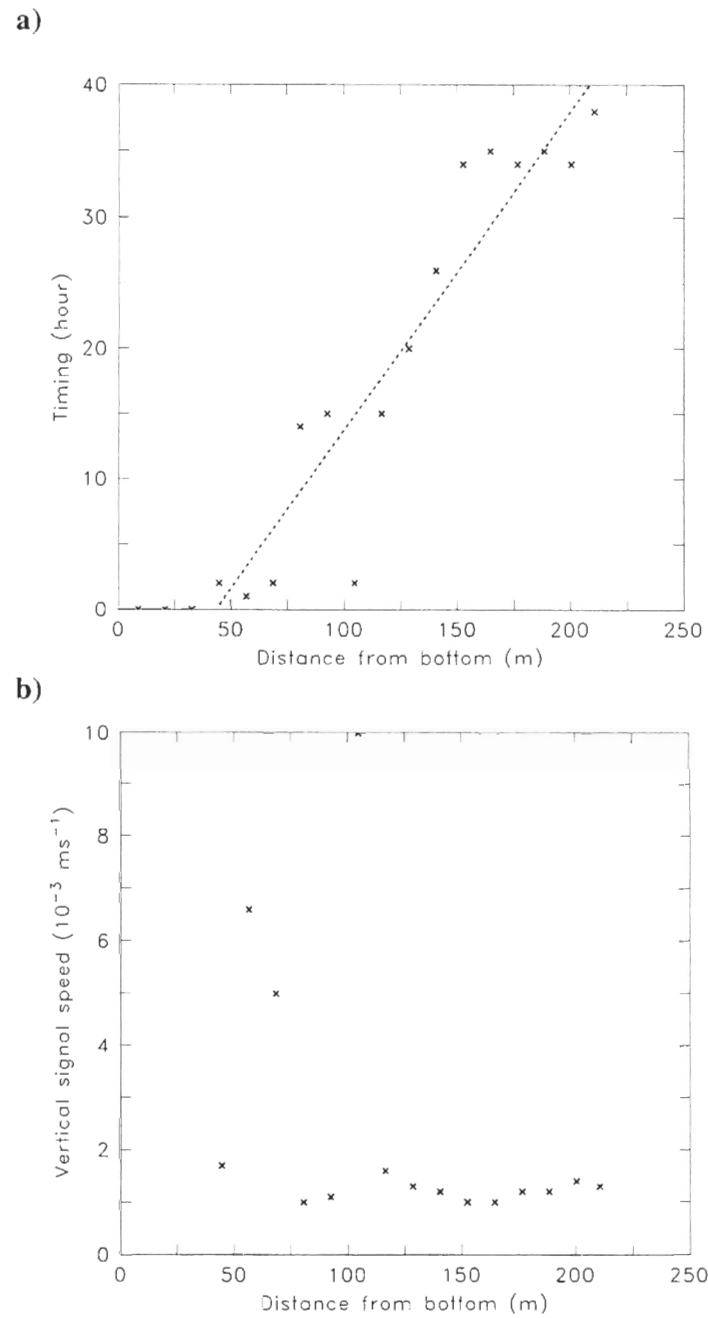


Fig. II.5. Vertical propagation of the dense water signal. **a** hours since first dense water signal detection; **b** dense water signal propagation speed (see Section II.2.2 for details on the calculation).

In Fig. II.6, the salinity time series at 150 m depth for the year 2004-2005 is drawn along the one at 360 m for comparison. Although it has been low-pass filtered in order to remove tidal frequencies, it shows more variability than the unfiltered curve at 360 m. This may be due to the influence of the HB intermediate water flowing into FC (*e.g.*, Jones and Anderson, 1994), although local vertical and lateral currents in the channel could also play a role here.

The T-S diagram in Fig. II.7 is used to estimate the percentage of mixing when the deep waters in FC are renewed by the new dense waters associated to the pulse. The temperature and salinity at the two end points P_1 and P_2 of the mixing line come from Fig. II.2. P_1 represents FC's deep water characteristics just before the abrupt temperature drop and salinity rise, while P_2 represents the incoming dense water characteristics. P_{M1} and P_{M2} correspond to the mixing of the deep waters at the end of the pulse and one month later, respectively. Note that P_{M2} is measured before any autumn storm may disrupt the water column in FB. The coordinates for P_1 , P_2 , P_{M1} and P_{M2} are summarized in Table II.1.

Note also that at the bottom of FC, the difference between the temperature T and the potential temperature θ is always smaller than 0.01 °C; for example, with $T = -1.84$ °C and $S = 33.75$ at 440 m, $\theta = -1.85$ °C. Despite this small difference, the temperature data have been converted to potential temperature when possible, *i.e.* in Fig. II.2a, II.7 and Table II.1. In Fig. II.3 and II.4, the temperature has not been converted since there is no salinity data available at the depth of the sensors.

2004 (mooring M8, 440 m depth)	date	θ (°C)	S
P_1	April 6	-1.64	33.26
P_2	May 9	-1.85	33.75
P_{M1}	June 30	-1.78	33.60
P_{M2}	July 31	-1.81	33.68
2005 (mooring M25 _a , 360 m depth)			
P_1	April 22	-1.62	33.33
P_2	May 20	-1.85	33.64
P_{M1}	September 9	-1.75	33.50
P_{M2}	October 9	-1.79	33.58

Table II.1. Characteristics of the T-S mixing lines at the bottom of Foxe Channel during the dense water pulse for the years 2004 and 2005. P_1 and P_2 are the end points of the lines. P_{M1} and P_{M2} are the mixing points just when the pulse stops and one month after, respectively.

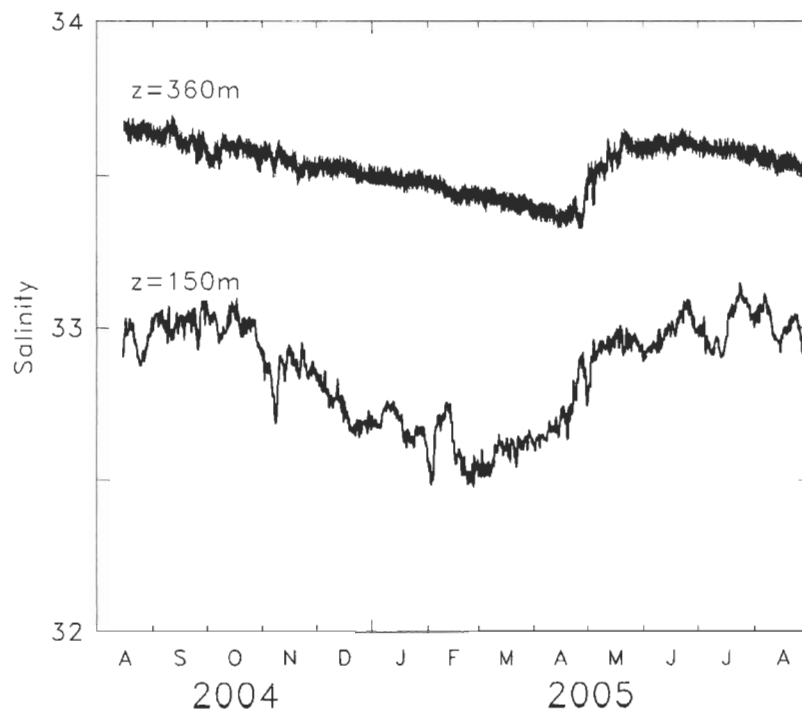


Fig. II.6. Comparison between the salinity at 360 and 150 m depth in Foxe Channel. The time series at 360 m uses the original data because their high frequency component is weak compared to the seasonal cycle while the one at 150 m is low-pass filtered in order to remove the tidal signal.

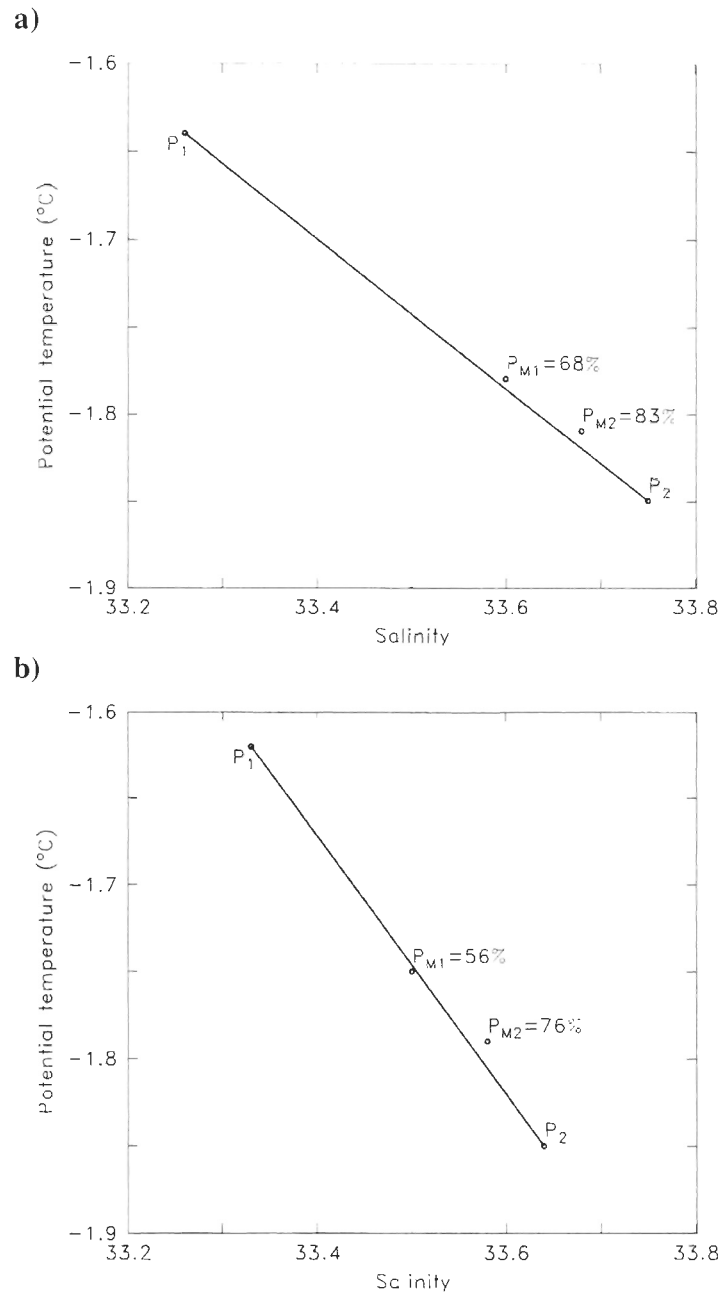


Fig. II.7. T-S diagram representing the mixing of Foxe Channel's deep waters with the incoming dense waters for 2004 (a) and 2005 (b). P_1 and P_2 are the deep water and new dense water characteristics, respectively. P_{M1} corresponds to the end of the dense water arrival while P_{M2} is measured one month later; the numbers beside represent the percentage of mixing.

II.3. DENSE WATER SPEED IN FOXE CHANNEL

II.3.1. Vertical propagation speed of the dense water signal

In order to understand the effect of the dense water pulse over the water column, it is useful to estimate the vertical propagation speed by detecting the signal emerging from the pulse at different depths. These quantities are taken and calculated from the temperature time series in Fig. II.3a; the results for the signal detection curve and the vertical propagation speed are shown in Fig. II.5a and b, respectively.

In Fig. II.5a, the arrival time of dense water increases nearly linearly. The regression line obtained from the least square method is: $t = 0.24 d - 10.55$, where t is the detection time in hours and d is the distance in meters from the top of the dense water layer when the signal is first detected; the correlation coefficient for this regression is $r^2 = 0.89$. Note that the top of the dense water layer is used instead of FC's bottom because the peak after the temperature drop for the series at 357, 345 and 333 m depth occurs at the same time (April 28, 2005 at 01 h UTC).

In Fig. II.5b, the vertical propagation speed is calculated as the ratio of the distance from the top of the dense water layer divided by the travel time of the signal. This calculation is in fact a time derivative that is sensitive to small inaccuracies in the data. For that reason, the values greater than $2 \cdot 10^{-3} \text{ ms}^{-1}$ are excluded and the mean vertical propagation speed of the dense water signal is $(1.25 \pm 0.22) \cdot 10^{-3} \text{ ms}^{-1}$ (it would be $(2.44 \pm 2.57) \cdot 10^{-3} \text{ ms}^{-1}$ if all values were retained). This speed, however, is not to be

mistaken for the thickening speed of the dense water layer which can be deduced from Fig. II.4: $140 \text{ m} / 26 \text{ days} \approx 5.4 \cdot 10^{-5} \text{ ms}^{-1}$. In other words, although the signal can be detected at the surface of FC at M25's position in less than 4 days ($360 \text{ m} / 1.24 \cdot 10^{-3} \text{ ms}^{-1}$), it takes at least 26 days to displace the isotherms 140 m towards the surface.

II.3.2. Calculation of horizontal mean speed of the dense water current

Fig. II.3a shows that there is a cold water mass lasting from February to March 2005 and above 180 m depth in FC. This cooling is coupled with an increase in salinity starting in February 2005 (Fig. II.6). These salty waters are probably due to the formation of ice and associated brine rejection in FB during winter. Since this cold surface layer never reaches the bottom of FC and the dense water signal propagates upwards, the dense water arrival in the channel may not result from a local deepening of the winter surface layer. Furthermore, Fig. II.2 shows that the dense water pulse is detected sooner in the year at mooring M8 (April 5) than at M25_{a,b} (April 22 in 2005 and May 22 in 2006), M25_{a,b} being located 93 km southeast of M8. The time lag between the pulse detection at M8 and M25_{a,b} is large enough to indicate that the dense water mass travels from the northeast of FC toward the southwest. This is coherent with the continuity of the deep water temperature and salinity (Fig. II.2a and b) seen at the beginning of August 2005. Also, the direction of this dense water circulation is in agreement with FC's mean cyclonic circulation. Therefore, the dense water pulse comes from a lateral advection of a water mass flowing southeastwards at the bottom of FC.

Although the observations do not provide any direct measurement of the dense

water current in FC, it is interesting to have at least an estimation of its horizontal speed. Kämpf's (2000) semi-empirical approximation of dense water along-slope velocity, which is valid for constant bottom slopes, provides a simple way to estimate this current:

$$\bar{v}_{dw} \approx 0.25 \frac{\rho_{dw} - \rho_{sw}}{\rho_{sw}} \frac{gs}{f} \quad (1)$$

where ρ_{dw} is the dense water density, ρ_{sw} is the surrounding water density, g is the gravity acceleration, s is the topographic slope and f the Coriolis parameter.

The characteristics of the dense water produced in FB can be obtained from Fig. II.2 by taking the minimum of potential temperature and maximum of salinity at 440 m during the pulse, *i.e.*: $T_{dw} = -1.85$ °C and $S_{dw} = 33.75$ and therefore $\rho_{dw} = 1029.28$ kg·m⁻³. Fig. II.2 gives also the characteristics of the surrounding water at the bottom of FC: $T_{sw} = -1.64$ °C, $S_{sw} = 33.27$ and $\rho_{sw} = 1028.88$ kg·m⁻³. The slope at the bottom of FC's deepest trough is $s \approx 2.4 \cdot 10^{-3}$. The Coriolis parameter at the latitude of 65.14 °N is $f = 1.32 \cdot 10^{-4}$ s⁻¹. With these values, Eq. 1 gives $\bar{v}_{dw} = 1.7 \cdot 10^{-2}$ ms⁻¹.

Note that this horizontal speed may be underestimated since the measurements and calculations are made in a trough, *i.e.* at a location where the topographic slope flattens. According to Ivanov *et al.* (2004), the dense water current in the channel is the result of a cascade. Due to the bathymetry, this cascade is likely to occur at the topographic break near Winter Island (WI), in southwestern FC. In this area, the value of the slope is $5 \cdot 10^{-3}$, which means that the maximal speed of the dense water current would be $3.6 \cdot 10^{-2}$ ms⁻¹.

II.4. DISCUSSION

II.4.1. Origin of the dense water mass detected at depth in Foxe Channel

The characteristics of the deep waters observed in 2004, 2005 and 2006 are similar to those reported in 1982 by Jones and Anderson (1994) who assume that they are unlikely to be renewed each year because they are trapped into the channel's depressions. However, the observation of the dense water pulse clearly contradicts this assumption. This raises the question about the origin of these waters: were they advected from the surrounding parts of FB or formed in the basin?

There are three possible pathways for a water mass to enter FB (see Fig. II.1a for locations): a) from the GB and flowing through FHS; b) from HS and passing through the complex formed by three small islands (Nottingham (NI), Salisbury Island and Military Island) and sills around 200 m depth; and c) from HB and overflowing either the sill at 180 m depth between Southampton Island (SI) and NI or the one at 50 m at northern RWS. Since the arctic waters entering FB via FHS are less dense than the waters already present in the basin (Prinsenber, 1986), the first hypothesis a) can be discarded and if arctic water is found at depth in FC, it must be through an *in-situ* convective process. Hypotheses b) and c) are quite similar because they both imply that dense water would have to flow over sills smaller than 200 m deep. However, they are not consistent with the description of the general circulation and density distribution given by Saucier *et al.* (2004a) and so hypotheses b) and c) are discarded too.

There are also three possibilities for *in-situ* dense water formation: d) concentration of brine-rich sea water repeatedly exposed to very cold winter air temperature ($< -35\text{ }^{\circ}\text{C}$) in eastern FB's tidal flats (Campbell, 1964); e) continuous brine rejection during the freezing of FB over the whole domain and sinking of the winter surface layer down to FC's bottom; and f) intense brine rejection and dense water production in western FB's latent heat coastal polynyas. Campbell's description seems plausible, however, neither the current nor the volume of dense water produced on the tidal flats can be large. In particular, these waters are likely to be trapped in ponds and their circulation impeded by fast ice close to the sea bottom. Furthermore, they would have to travel 700-800 km, according to FB's cyclonic circulation, without losing density through mixing with surrounding waters in order to reach FC's deepest depression. Since the maximum current values estimated at depth in FB are generally less than 10^{-1} ms^{-1} (Saucier *et al.*, 2004a), this means that the dense waters should have been produced more than three months before reaching the trough at the beginning of April, *i.e.* before the start of winter or during early winter, which is quite improbable and thus hypothesis d) is rejected. Hypothesis e) cannot be retained either because the continuous brine rejection during the freezing of FB is a progressive process that is not consistent with the pulse-like propagation of the dense water signal. This would only lead to the deepening of the winter surface layer, though not enough to reach the bottom of FC (see Section II.3.2). Therefore, the only hypothesis left is f) and the following paragraphs are meant to further investigate its validity.

The pattern of the temperature and salinity time series in Fig. II.2 shows that the characteristics of the incoming dense waters distinguish them well from the surroundings

waters. This observation can be exploited in order to attempt to trace the origin of the dense waters by using a simple backtracking procedure and the current field obtained from a numerical model. The detailed description of the ice-ocean model is found in Saucier *et al.* (2004a); it is a z-level, hydrostatic, shallow water, incompressible formulation and is coupled to a dynamic and thermodynamic two-layer sea-ice and one-layer snow cover model. The vector field is extracted from a $10 \text{ km} \times 10 \text{ km}$ horizontal grid with a vertical resolution varying from 10 m at the surface to 50 m at the bottom of FC and is averaged over a 3 hours period (the numerical model uses a time step of 5 minutes). The procedure consists in filling a small virtual volume of water at the bottom of the channel with Lagrangian tracers and to follow their trajectories back in time, assuming negligible effects from mixing. Initially, on May 9, 2004, the volume of water is defined by a 0.1 m diameter sphere, *i.e.* small compared to the layer thickness of the water column, whose position and depth correspond to mooring M8's location.

In Fig. II.8a, the Lagrangian tracers flow globally southwards and their trajectories can be divided into two parts: from HaB to Lyon Inlet (LI); and from LI to FC's deepest depression at 450 m. Note that as long as the tracers mark the dense waters during the pulse, their trajectories vary little when their initial position and/or date are modified. The backtracking procedure is therefore robust when the dense water mass is well distinguished from the surrounding waters. Fig. II.8a also shows that the bottom current in the shallow channel along the eastern coast of MP clearly accelerates at the topographic break in the vicinity of WI. This is in accordance with the dense water cascade described by Ivanov *et al.* (2004).

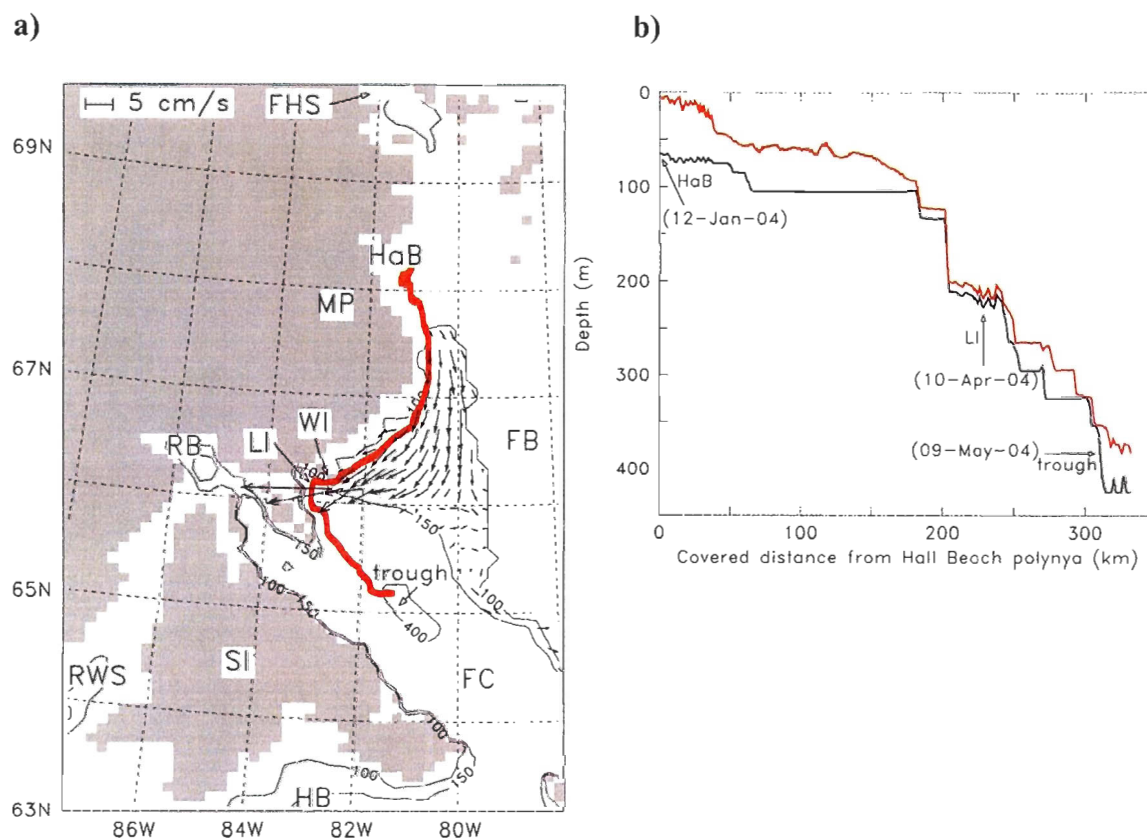


Fig. II.8. Dense water circulation and cascade in Foxe Basin. In **a**, the red curve shows the trajectory of Lagrangian tracers backtracking in time the dense water mass. The vector field represents the bottom current in the shallow channel along Melville Peninsula, the scale is in the upper left of the figure. In **b**, the red curve shows the vertical displacement of the tracers as a function of the covered distance. The black curve represents the bottom of the basin. The arrows point to the location of the polynyas at Hall Beach and in Lyon Inlet, and to the location of the deepest trough in Foxe Channel. The dates in brackets correspond to the tracers' position. (see Fig. II.1 for acronyms definitions)

In Fig. II.8b, the vertical displacement of the tracers shows that the dense waters which cascade into FC come originally from the sea surface at HaB and that this cascade occurs at LI. The mean tracer speed is $2.9 \cdot 10^{-2} \text{ ms}^{-1}$ between HaB and LI (225 km / (April 10 - January 12)) and $4.4 \cdot 10^{-2} \text{ ms}^{-1}$ between LI and FC's deepest trough (110 km / (May 09 - April 10)). These values are higher than those estimated above in Section II.3.2 which is not surprising since the tracers flow along one stream line while Kämpf's formula applies to the bulk water mass. It is important to note that north of HaB, the backtracking procedure is not valid since the dense waters have not yet been formed and that the tracers can come from anywhere in northern FB; this is why the trajectory is ended at HaB in Fig. II.8.

When compared with the satellite image taken during winter (Fig. II.9), it is clear that the path followed by the Lagrangian tracers follow closely the location of western FB's polynyas at HaB, along MP and in LI. This is a strong indication that the dense waters found at depth in FC originate from these polynyas and that hypothesis f) is therefore supported by the observations. Thus, the results of our numerical experiment suggest that the dense water current is the result of brine rejection in HaB's polynya and along MP; this brine flows southwards then southwestwards until the topographic break where it cascades into FC and can combine with the dense waters produced in LI's polynya. Note that at LI's polynya, dense waters can sink directly at the bottom of the channel through deep convection because of greater depths. Further work involving the polynyas' dynamics, heat exchanges with the atmosphere and dense water production will be necessary to examine the pulse-like propagation of the gravity current at the bottom of the channel.

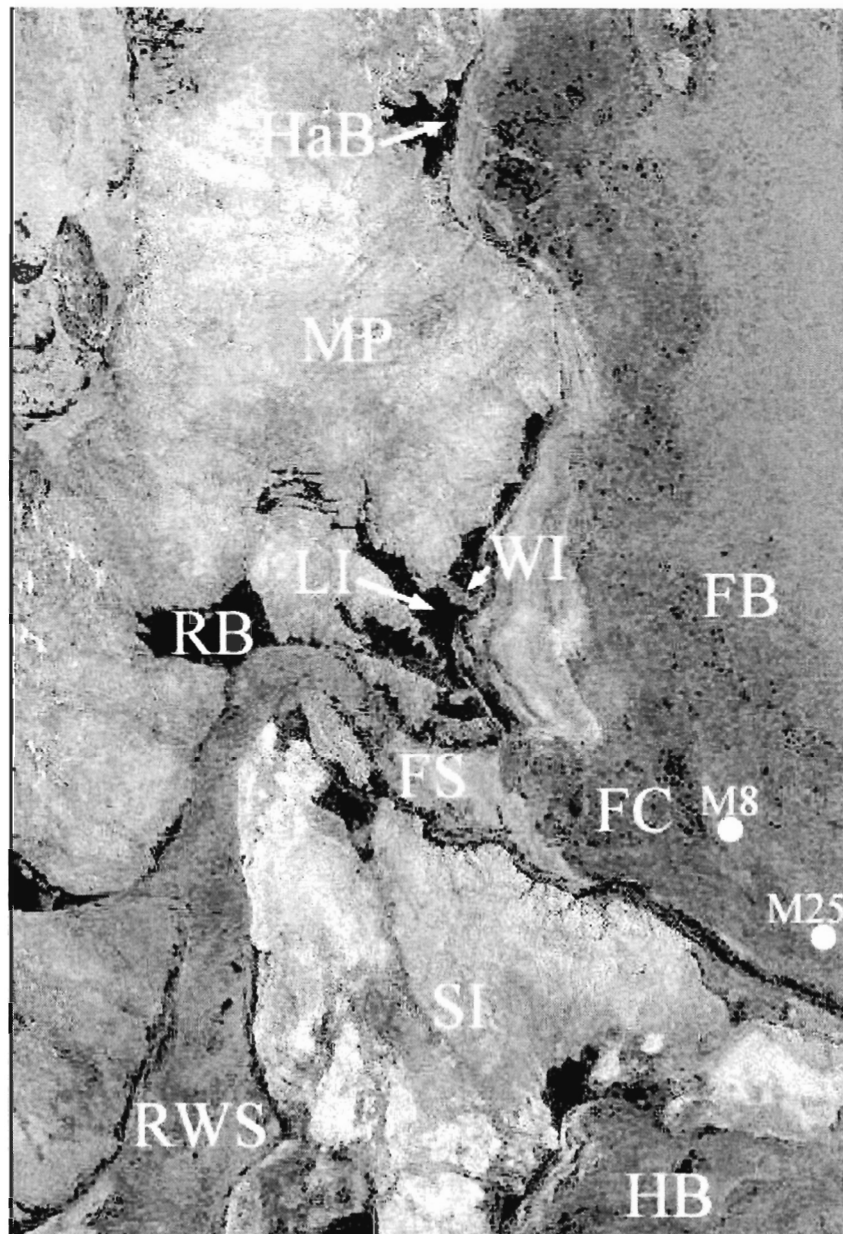


Fig. II.9. Satellite image showing the sea-ice distribution on March 4, 2004, over western Foxe Basin (European Space Agency, Envisat ASAR Wide Swath). The polynyas (ice free areas) appear in black while the sea-ice is light grey. The locations of the moorings M8 and M25 are indicated with white dots (see Fig. II.1 for acronyms definitions).

Note also that the characteristics of the dense waters produced in FB differ significantly from those found in the Arctic Mediterranean at a depth of around 500 m and described by Aagaard *et al.* (1985): they are generally colder ($-1.85\text{ }^{\circ}\text{C}$ vs. $0\text{ }^{\circ}\text{C}$) and fresher (33.75 vs. 34.8).

II.4.2. Recurrence of the dense water pulse at the bottom of Foxe Channel

The dense water pulse observed consecutively from 2004 to 2006 shows a strong seasonal cycle associated with lesser interannual variability at the bottom of FC (Fig. II.2). By taking 2004 as a reference year, the seasonal cycle can be roughly divided into three intervals: a) An abrupt arrival of dense water starting at the beginning of April and characterized by a temperature drop from $-1.64\text{ }^{\circ}\text{C}$ to $-1.85\text{ }^{\circ}\text{C}$ over five days and by a salinity rise from 33.27 to 33.75 over one month; b) A two month period over which a near freezing and saline water mass flows through FC's deepest trough with no significant change of its properties. This period ends with a sharp rise in temperature indicating that the current no longer has enough kinetic energy to drive the deep waters away and that some mixed water reenters the trough; and c) A progressive warming and freshening of the deep waters during fall and winter. This description is still valid for the year 2005, although the end of the pulse is not as abrupt as in 2004 which may be due to the fact that the mooring M8 was in a trough while M25_{a, b} was on a slope at a lesser depth. For 2006, the salinity data are not complete but it can be seen that the pulse in temperature is shorter (2 months) and that it starts with a delay of one month compared to the one in 2005, that is: May 22 rather than April 22.

The occurrence of cold saline water in FC was first reported for the years 1955 and 1956 by Campbell (1964) who suggested that it was sporadic because no such dense water was found in the following surveys. It must be noted, however, that Campbell's observations were not based on time series but on oceanographic stations located roughly along the 80 °W from Hall Beach (HaB) to southern FC. Since the dense water pulse lasts approximately three months and travels southeastwards along the channel, it can be easily missed by a non-continuous measure of the deep water characteristics. Furthermore, the pulse was significantly less marked in 2006. The winter in FB was approximately five degrees warmer than for the two previous years: the air temperature at RB meteorological station averaged from December 20 to March 20 was -31.8 °C in 2003-2004, -32.1 °C in 2005 and -27.0 °C in 2006. The mean winter temperature in this region is -30.6 °C for the period 1984-2006, making 2005-2006 a particularly mild winter. Since the new dense waters are produced in western FB's polynyas, this can explain the differences observed between the 2004 and 2005 dense water pulses. The deep water renewal in FC seems therefore strongly dependent on the severity of the preceding winter, that is, the atmosphere controls the dense water production in FB. Fig. II.2a shows also that the fluctuations in temperature at the bottom of FC are greater in 2006 than in 2004 and 2005, and that the temperature during the pulse is 0.07 °C above the freezing point. This may be due to an increase in the vertical mixing facilitated by a thinner or less extensive sea-ice cover since, in that case, the effect of the wind stress and the sensible heat loss to the atmosphere could be greater, both phenomena acting on the water column stability. This also indicates that FC's deep waters are still renewed even during a mild winter and therefore that the dense

water pulse observed at the bottom of FC is a permanent characteristic of the seasonal cycle.

Interestingly, Fig. II.2b shows clearly that during the deep water renewal event, the salinity reaches two consecutive peaks with a difference of 69 days (July 14 and May 6) in 2004 and 122 days (September 21 and May 22) in 2005. For both years, the second peak in salinity corresponds to a sharp increase in temperature from $-1.85\text{ }^{\circ}\text{C}$ to $-1.78\text{ }^{\circ}\text{C}$ in 2004 and from $-1.85\text{ }^{\circ}\text{C}$ to $-1.75\text{ }^{\circ}\text{C}$ in 2005 (Fig. II.2a). Since the dense waters are likely formed by the abrupt cooling of surface waters in western FB's polynyas, this temperature rise excludes the possibility of a secondary pulse. This rather suggests that when the pulse stops, the bottom of the water column restratifies, allowing back some of the dense water. The same water mass, although partially mixed with deep waters, is therefore observed again.

The percentage of deep water renewed in FC by the new dense waters arriving at the bottom of the channel can be estimated from the temperature and salinity values of these two water masses and with the help of the mixing line defined by $P_{1,2}$ and P_{M_1,M_2} (Table II.1). For 2004 (mooring M8, Fig. II.7a), when the calculation is made as soon as the pulse stops (June 30, 2004), one finds that 68 % of the deep waters are renewed. When the same calculation is made one month after the pulse (July 31, 2004), the result is 83 %. Note that P_{M_1} is close to the mixing line, thus confirming the presence of two distinct water masses at the bottom of FC: the deep waters formed during the previous winter and the newly advected dense waters. Note also that P_{M_2} is somewhat beside this line which may be due to some mixing with surrounding waters. In both cases, these high percentages show

that the pulse is an energetic event that is able to mix the water masses at depth. For 2005 (mooring M25_a, Fig. II.7b), the calculation of the deep water renewal when the pulse stops and one month after gives 56 % and 76 %, respectively.

Note that since around $2/3^{\text{rd}}$ of the deep waters in FC are renewed each year, the remaining dense water volume V_{dw} of an initial volume V_{dw0} after n years is:

$$V_{dw} = V_{dw0} \left(1 - \frac{2}{3}\right)^n \quad (2)$$

By analogy with an exponential decay law, Eq. 2 can be rewritten as:

$$V_{dw} = V_{dw0} e^{-\frac{n}{\tau}}, \quad \tau = \frac{1}{\ln(3)} \quad (3)$$

where $\tau \approx 0.9$ year is the characteristic turnover time of the system.

These results are important because, except for the pulse, the fluctuations in water characteristics at the bottom of FC are weak. Therefore, the pulse of dense water at the bottom of FC is a major event that each year renews most of the channel's deep waters.

II.4.3. Effect of the dense water circulation on the water column in Foxe Channel

The effect of the pulse on the water column can be seen both in temperature and salinity. As from April 22, 2005, which corresponds to the arrival of the new dense waters at the bottom of FC, the temperature drops over the bottom 180 m of the water column, and there is a break in the slope of the salinity rise at 150 m depth. In Fig. II.3a, another interesting phenomenon happens in April 2005 between depths of 285 m and 180 m where a small temperature surge corresponding to an intrusion of intermediate water, either from

HB or Hudson Strait (HS), can be seen. Furthermore, the salinity difference in Fig. II.6 between the bottom of the channel and 150 m depth, *i.e.* below the bottom of FB's northern shelf, exceeds 0.5 all year long. This feature clearly distinguishes FC's deep waters from the other water masses in the basin. This also strengthens the hypothesis that the dense waters are formed through a particularly strong freezing process, *i.e.* that the dense water gravity current originates from FB's polynyas.

Despite a positive bottom slope from mooring M8 to M25 (440 m depth to 360 m), the dense water mass travels southeastwards in FC. This indicates that the dense waters must store a large amount of kinetic energy as they are formed. Therefore, the water column over the whole length of FC is likely to be affected by the dense water pulse when it propagates along the channel. This is also consistent with Saucier *et al.* (2004a) who found numerically that some of the dense waters may be able to overflow the sill at 180 m depth between SI and NI.

By forming a wedge below the water column in FC, the dense water intrusion tends to push the isopycnals upwards. For example, the temperature just before the pulse at 310 m depth is equal to $-1.6\text{ }^{\circ}\text{C}$ while after the pulse this same temperature is found at 175 m (Fig. II.3b). Although salinity data would be needed to ensure that the water mass at 175 m depth comes from the one at 310 m, this suggests a vertical displacement of around 135 m for the isopycnals at depth in FC.

Since it takes 26 days for the dense water mass to attain its maximal thickness of 140 m (see 3.1), there is a time lag of around one month for the whole water column to respond to the pulse. Fig. II.3b shows the dramatic effect of the deep water renewal: before

the pulse, the bottom layer is around 50 m thick and, one month later, it is completely replaced by the 140 m thick colder layer up to 220 m depth. Above that depth, the water column is more stratified. When the new dense waters fill the bottom of FC, currents tending to rebalance the water column must be induced by the rise of the isopycnals in the channel.

II.5. CONCLUSION

This study has shown that FC's deep waters are rapidly renewed each winter through the lateral advection of a cold and saline water mass. The deep water renewal has been observed in 2004, 2005 and, although the air temperature of the winter 2006 was approximately 5 °C warmer than the two previous ones, also in 2006. This indicates that the renewal is a strong component of the seasonal variability. Furthermore, the temperature at depth during the pulse was equal to the freezing point taken at the surface of the sea in 2004 and 2005, while it was 0.07 °C above the freezing point in 2006. Since the dense waters seen at depth in FC are likely produced in western FB's coastal polynyas, this shows that the variability in the characteristics of the dense water mass depends on the severity of the winter over the basin.

The dense water current flows southeastwards along the bottom of FC with an estimated speed of $1.7 \cdot 10^{-2} \text{ ms}^{-1}$. It is detected at depth by a sharp drop in temperature of 0.2 °C over five days and a rise in salinity of 0.5 over one month, and it lasts around three months. The water column responds to the dense water pulse with a time lag of one month. During this period, FC's bottom layer thickens from 50 to 140 m and the isotherms are raised accordingly. The mixing lines drawn from the characteristics of the deep waters before and during the pulse show that the newly advected dense waters generally mix and renew more than $2/3^{\text{rd}}$ of the deep waters at the bottom of the channel.

The aim of this work was to report the yearly recurrence of the deep water renewal

in FC, and to show that it is part of a seasonal cycle involving dense water production in western FB's polynyas. These results have both physical and biological significance since the dense water pulse affects the circulation in FC and ensures the ventilation at depth by bringing cold and saline waters formed at the surface to the bottom of the channel. Furthermore, as some of these dense waters may overflow into HB, it is important to study the consequences of the deep water renewal in FC on the general circulation in the whole HB system, especially in the context of climate changes. The mechanisms responsible for the pulse-like propagation of the dense water mass along FC, as well as the estimation of the dense water volume produced in the polynyas and its dependence with the atmospheric climate, will be addressed in the future.

**III. ANALYSIS OF A DENSE WATER PULSE FOLLOWING MID-WINTER
OPENING OF POLYNYAS IN WESTERN FOXE BASIN, CANADA**

ABSTRACT

A recent study has shown that Foxe Basin's dense waters originate from coastal latent heat polynyas and each year replace $2/3^{\text{rd}}$ of the basin's deep waters by propagating southeastwards in Foxe Channel as a gravity current. The formation mechanisms in 2004 of these dense waters are examined here. Strong meteorological events occurring in mid-winter over the domain are responsible for the simultaneous opening of two large polynyas at Lyon Inlet and along Melville Peninsula's eastern coast while a third important and recurrent polynya opens earlier at Hall Beach (northwestern Foxe Basin). Large sea-atmosphere heat exchanges take place in these polynyas, leading to the production of 21.2×10^{12} kg of sea-ice and 1.53×10^{12} m³ of dense water. The ice production rate is on average five to six times higher in the polynyas than in the rest of the basin. Following the topography, the dense waters formed at Hall Beach and along Melville Peninsula cascade into Foxe Channel, while those produced at Lyon Inlet sink directly in the channel through deep convection. The two mechanisms synchronize and combine together when Lyon Inlet and Melville Peninsula polynyas open up. The heat exchanges, sea-ice and brine production rates estimated with a 21 year near-climatology are similar to those found in 2004. The results also show that the produced dense waters can overflow into Hudson Bay.

III.1. INTRODUCTION

Continental shelves in polar regions produce large amounts of brine rich dense waters. Using two different methods (the first based on the residence time and thickness of the upper part of the pycnocline and the second on the transformation of Atlantic water in the Arctic), Aagaard *et al.* (1981) estimated that around 2.5 Sv ($1 \text{ Sv} \equiv 10^6 \text{ m}^3\text{s}^{-1}$) of dense water is produced on the shelves and contributes to the maintenance of the cold upper halocline in the Arctic Ocean. This halocline also helps to shield the ice cover from the heat flux of the warmer and saltier underlying water coming from the Atlantic, and the dense water therefore interacts indirectly with the thermohaline circulation in the northern Atlantic. Cavalieri and Martin (1994) studied the heat losses, ice and salt production specifically in the Arctic coastal polynyas and found that their contribution to the halocline is significant and lies between 0.7-1.2 Sv. In order to understand the impact of global warming in polar regions, it is therefore necessary to carry out detailed surveys of Arctic polynyas, including those located in adjacent seas, since they are by nature very sensitive to climate change.

It is in this context that the program MERs Intérieures du Canada (MERICA, Saucier *et al.*, 2004b) was initiated in 2003. It is funded by the Department of Fisheries and Oceans, Canada, and involves the long term monitoring of the climate variability and biological productivity of the Hudson Bay system (Fig. III.1a), consisting of three large Arctic marginal seas: Hudson Bay (HB), Foxe Basin (FB, detailed map in Fig. III.1b) and

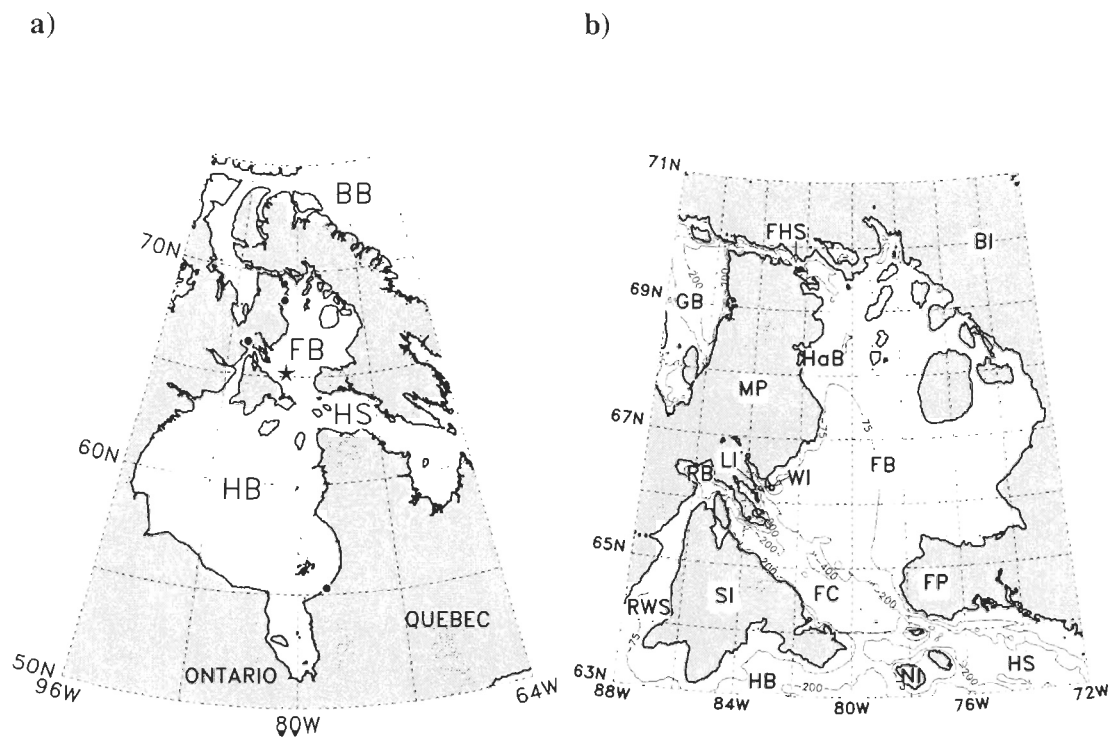


Fig. III.1. Hudson Bay system (a) and Foxe Basin (b). The isobaths come from ETOPO2 (NOAA). On a, the star indicates the mooring, and the black dots locate, from north to south, weather stations in Hall Beach, Repulse Bay and Kuujjuarapik. BB stands for Baffin Bay, BI for Baffin Island, FB for Foxe Basin, FC for Foxe Channel, FHS for Fury and Hecla Strait, FP for Foxe Peninsula, GB for Gulf of Boothia, HaB for Hall Beach, HB for Hudson Bay, HS for Hudson Strait, LI for Lyon Inlet, MP for Melville Peninsula, NI for Nottingham Island, RB for Repulse Bay, RWS for Roes Welcome Sound, SI for Southampton Island and WI for Winter Island.

Hudson Strait. The most comprehensive review to date of the oceanography of this system is found in Prinsenberg (1986); more recently, Saucier *et al.* (2004a) modeled its general sea-ice and ocean circulation.

FB is located north of HB and is crossed by the Arctic Polar Circle (66.56 °N). The basin is connected to the Arctic via the Gulf of Boothia and Fury and Hecla Strait, to HB via Roes Welcome Sound and the fairway between Southampton Island and Nottingham Island, and to the Labrador Sea via Hudson Strait. Foxe Channel (FC) is the deepest depression of FB; it is a straight channel approximately 400 km long and 100 km wide, with a maximal depth of 450 m, that follows Southampton Island's northern coast for most of its length. Table III.1 summarizes some of FB's main characteristics.

For three consecutive winters, 2004 to 2006, an abrupt arrival of cold and saline waters at the bottom of FC was observed by Defossez *et al.* (2008). These authors have shown that this gravity current is responsible for the renewal of more than 2/3rd of the channel's deep waters each year. Using Lagrangian tracers, they have also shown that the dense water forming this current comes from the sea surface in the vicinity of Hall Beach (HaB, Fig. III.1b), skirts along Melville Peninsula (MP) and then cascades into FC. The trajectory of the gravity current corresponds well to the location of three polynyas commonly found at western FB in winter: at HaB, along MP and at Lyon Inlet (LI). This indicates that the dense water observed at depth in FC is likely produced in these three polynyas and all what follows will therefore rely on this assumption.

The aim of this study is to provide a quantitative analysis based on oceanographic, meteorological and satellite data in order to explain the mechanisms leading to the pulse-

surface area (m ²)	mean depth (m)	maximal depth (m)	volume (m ³)	volume (depth>220 m) (m ³)
0.2×10 ¹²	90	450	18×10 ¹²	1.4×10 ¹²

Table III.1. Main topographic elements of Foxe Basin (based on ETOPO2, NOAA). The volume deeper than 220 m depth represents an overestimation of Foxe Channel's deep waters (see Section III.3.2.2).

like propagation of the dense water mass at the bottom of FC. The observations and data processing are described in Section III.2. These data allow the calculation in Section III.3 of heat exchanges arising at the sea-atmosphere interface of western FB's polynyas and thence, of the amount of ice and dense water produced yearly. The results are discussed in Section III.4, with a special emphasis on the relationship between atmospheric events occurring in mid-winter, polynyas opening and the dense water pulse detection at the bottom of FC. The consequences on FB's circulation are also discussed. The conclusion of this paper is given in Section III.5.

III.2. DATA DESCRIPTION AND METHOD

III.2.1. Oceanographic and meteorological data

The oceanographic data come from a mooring (Fig. III.1a) deployed from August 2003 to August 2004 as part of the MERICA program. Its position was 65.14 °N and 81.34 °W and it was moored at 440 m depth at the bottom of FC. Note that the location of the mooring corresponds to the deepest trough in FC, roughly in the middle of the channel.

The instrument installed on the mooring was a CTD (Conductivity Temperature Depth, SBE-19 from Sea-Bird Electronics) that recorded the water temperature and the salinity at the bottom of FC for one year. The sampling rate of the CTD was set to 15 minutes; the precision and resolution of the sensors were, respectively, 10^{-3} and 10^{-4} Sm^{-1} in conductivity, and 10^{-2} and 10^{-3} °C in temperature.

Fig. III.2a shows the time series obtained at depth in FC. The potential temperature and the salinity are plotted on the same graph in order to emphasize the synchronism between these two physical quantities when the cold and saline water mass is detected at the bottom of the channel. Note that the temperature drop from -1.64 to -1.85 °C takes only five days (April 4-5 to April 8-9, 2004) while the salinity rise from 33.27 to 33.75 takes approximately one month (April 5-6 to May 9-10, 2004). The discrepancy between the two transition speeds is not easy to interpret in the absence of a direct measurement of the gravity current. It may result from the fact that the cooling of surface water in the polynyas is faster than the frazil ice generation because this cooling alone is practically sufficient to

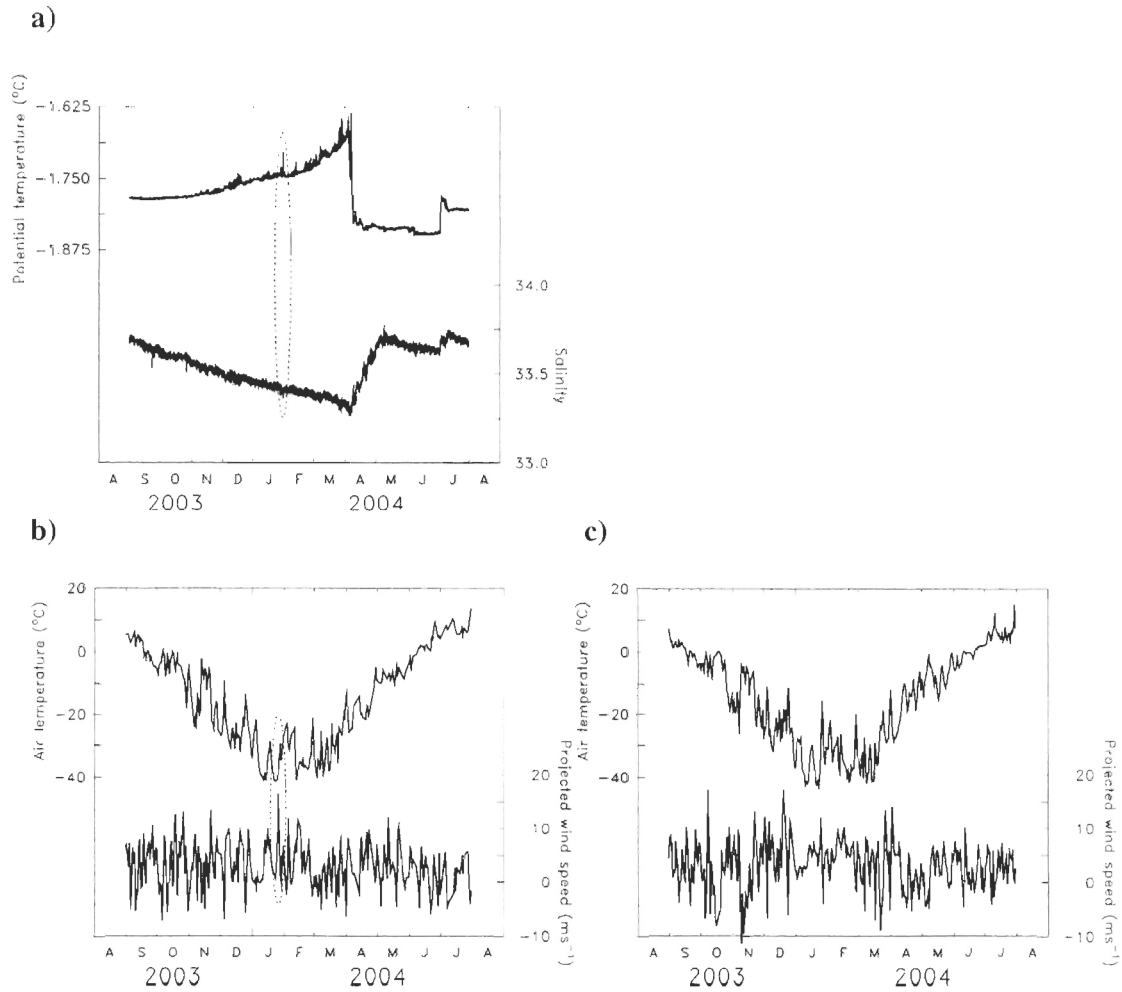


Fig. III.2. Foxe Channel's deep water response to sea-surface atmospheric events. The time series for the water characteristics at 440 m depth is drawn in **a**, while the ones for the meteorological parameters at Repulse Bay and Hall Beach weather stations are drawn in **b**, and **c**, respectively. The projected wind speed represents the positive southeastward component of the wind. The ellipses highlight the effect of the mid-winter peak in wind and air temperature on the deep waters.

induce the sinking of the surface water to the bottom of FC. This can be explained by comparing the density $\rho(S, T (\text{°C}), z (\text{m}))$ just before the pulse and five days (April 9) after its start when the salinity has only increased by 0.08 from 33.27 to reach 33.35: $\rho(33.27, -1.64, 440) = 1028.88 \text{ kg m}^{-3}$ while $\rho(33.35, -1.85, 440) = 1028.96 \text{ kg m}^{-3}$. In other words, although the incoming water is not yet very saline at the beginning of the pulse, it is already denser than the deep water. The discrepancy, however, may also result from a delayed release of salt in the water column when grease ice and pancake ice, formed at the polynyas' surface, expel saline water caught in their mass while being compacted with the ice sheet.

The local peaks in temperature and salinity (January 29, 2004) indicated by the ellipse drawn in Fig. III.2a are likely the response, within 3 to 4 days, of the deep water characteristics in FC to the peak of northwesterly winds (January 26, 2004) blowing over the channel (Fig. III.2b). The downwards propagation of this signal is then between 1.3 and $1.7 \times 10^{-3} \text{ ms}^{-1}$ (440 m / 4 or 3 days). A correspondence between similar mid-winter atmospheric events and ocean response has been observed in 2005 (not shown). Furthermore, Defossez *et al.* (2008) estimated that the signal emerging from the dense water pulse detected at the bottom of FC propagates vertically at around $1.25 \times 10^{-3} \text{ ms}^{-1}$, this suggests that the vertical propagation speed of the signal coming from a single strong event in the channel is the same whether it travels downwards or upwards. The 2004 peak in wind speed will be used as starting point in order to estimate the mean gravity current speed at the bottom of the channel (see Section III.4.1). Note that these strong winds lead eventually to the opening of western FB's polynyas.

The meteorological data at Repulse Bay (RB), HaB and Kuujjuarapik weather stations have been obtained from the Environment Canada database. The air temperature, wind speed and direction come from hourly data reports ranging from 1984 to 2006. All measurements have been acquired at 10 m height. The wind intensity and direction are not shown in this study; the projection of the wind speed on an axis parallel to FC in the southeastward direction is drawn instead because this is the component that tends to push the ice floes off the eastern coast of MP.

The altitude of RB weather station is 24.4 m and it is located at southwestern FB (66.52 °N and 86.22 °W, Fig. III.1a). It is the nearest station from LI and MP's polynyas (approximately 120 km). It is manually operated and, as a consequence, the data are mostly available during daytime and at times sparse. The resulting gaps have been filled by barycentric extrapolation centered at noon each day. The biases due to the lack of nighttime data have been estimated and corrected with the help of data from the closest and downwind automated station (Coral Harbour on Southampton Island, 291 km from RB).

The altitude of HaB weather station is 8.2 m and it is located at northwestern FB (68.78 °N and 81.24 °W, Fig. III.1a). This station is next to HaB's polynya and 327 km north of RB. Although it is automated, the data have also been extrapolated at noon each day for consistency reason with RB's data; no correction was needed in this case.

Additionally, meteorological data from the automated Kuujjuarapik weather station have been used to supplement the discussion on atmospheric pressure effects in Section III.4.3. This station is located at southeastern HB (10.4 m altitude, 55.28 °N and 77.75°W, 1327 km south of RB, Fig. III.1a). Here again the data have been extrapolated at

noon without further correction.

Long term weather conditions are also used here with data averaged over a 21 year period (1984-2006). Although this period is not long enough to qualify as a climatology, this naming will be used in the rest of the text for simplification. The result is shown along with the standard deviation (SD) in Fig. III.3a-d. By removing the interannual fluctuations, this climatology features the prominent aspects of the atmospheric seasonal cycle in this Arctic/Subarctic region, especially in February when FB's southwestern polynyas open up.

III.2.2. Satellite data

In order to calculate the dense water production in western FB's polynyas, it is necessary to examine the main parameters pertaining to their dynamics, *i.e.*, their location, surface area and downwind width as a function of time. Yackel *et al.* (2001) pointed out that satellite data obtained from synthetic aperture radars (SAR) were useful tools to estimate changes in polynyas because of their resolution (tens to hundreds of meters) and their insensitivity to cloud cover as well as to polar darkness. Thus data from the European Space Agency's (ESA) Envisat mission (advanced SAR sensor, wide swath mode: 400 km) have been used in this study. Although the Envisat satellite covers the whole HB system regularly, there are few available archived images for the region of interest near western FB. However, for the year 2004, it has been possible to retrieve data showing the ice distribution before (January 6 at 03 h UTC, Fig. III.4a) and after (March 4 at 16 h 15 UTC, Fig. III.4b) the opening of the polynyas. In Fig. III.4, the contrast of the images has been enhanced so that open water areas appear black while sea-ice covered areas are light-grey.

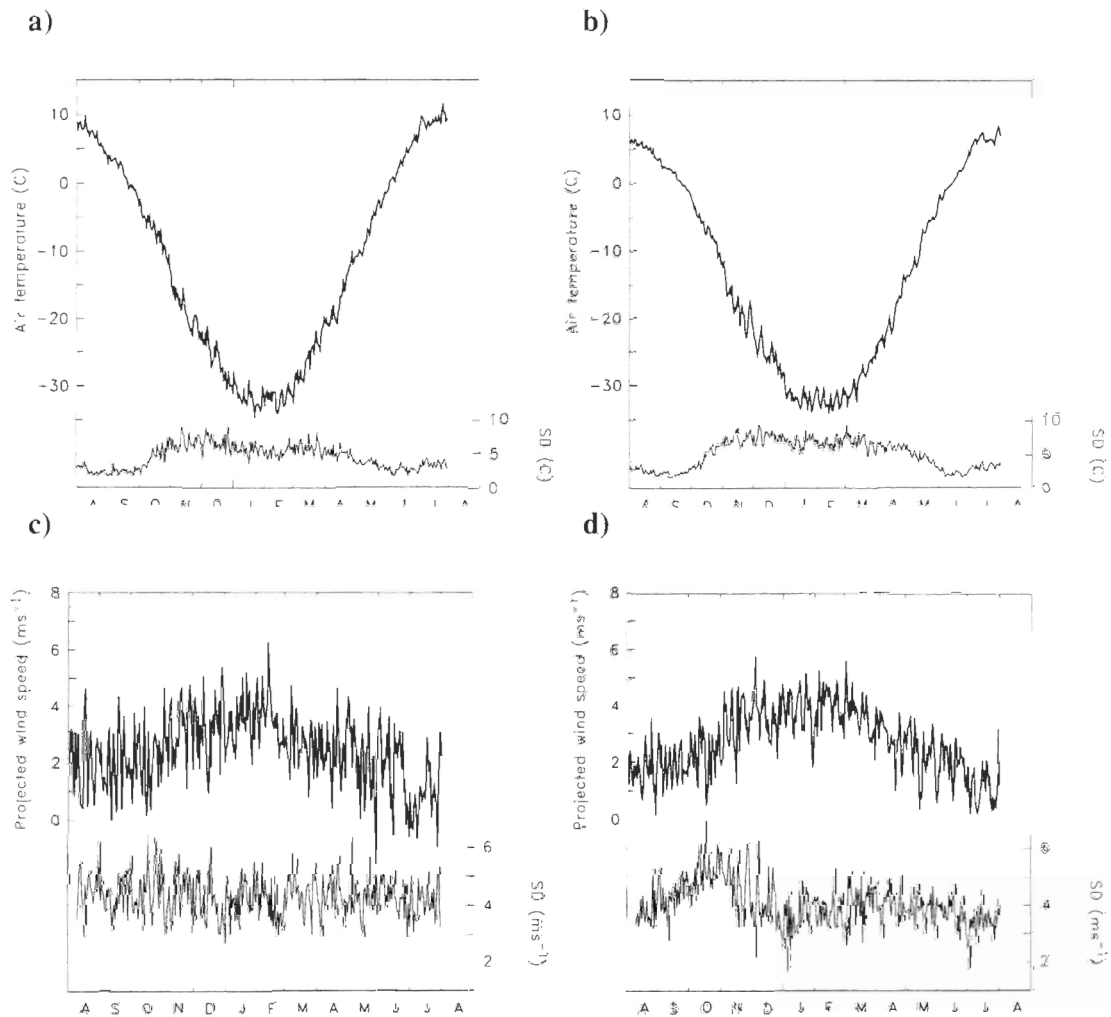


Fig. III.3. Atmospheric parameters averaged from 1984 to 2006 at Repulse Bay (**a**, **c**) and Hall Beach (**b**, **d**) weather stations. The air temperature is drawn in **a** and **b** while the southeastward wind component is drawn in **c** and **d**. The thick lines represent the averaged value and the thin lines the standard deviation (SD).

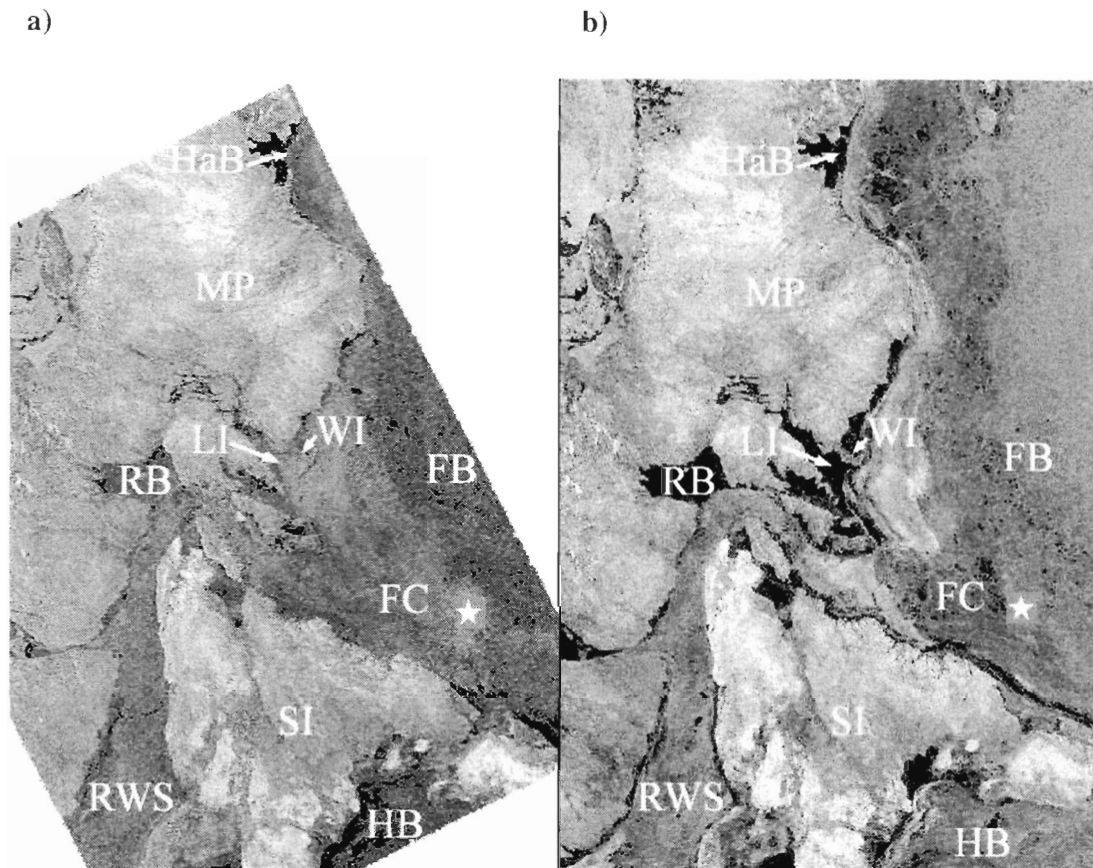


Fig. III.4. Satellite images (European Space Agency, Envisat ASAR Wide Swath) showing the opening of polynyas in western Foxe Basin. **a** and **b** were acquired on January 6, 2004 and March 4, 2004, respectively. The polynyas appear in black while the sea-ice is light grey. The location of the mooring is indicated with the white star (see Fig. III.1 for acronyms definitions).

The open water surface area as a function of time obtained from the satellite images is noted $A(t)$. For LI and MP's polynyas, which open up in mid-winter, it is defined as a linear function:

$$\begin{cases} A(t < t_1) = 0 \\ A(t > t_2) = A_{\max} \\ A(t_1 \leq t \leq t_2) = \frac{(t - t_1)}{(t_2 - t_1)} A_{\max} \end{cases} \quad (1a)$$

where A_{\max} is the surface area of the fully open polynya, and with $t_1 =$ January 1 (when the polynyas start to open) and $t_2 =$ March 1 (when the polynyas are fully open and remain so afterwards). For HaB's polynya, which can be considered continuously open during the winter, the function is simply:

$$A(t) = A_{\max}, \quad \forall t \quad (1b)$$

The dynamics defined by Eq. 1 is quite straightforward and does not account for the formation of thin ice that may occasionally impede the heat transfers at the polynyas' surface. The mean value of the projected winds between t_1 and t_2 is $(4.3 \pm 3.5) \text{ ms}^{-1}$, which indicates that they sometimes may not have enough strength to maintain the polynyas fully open. However, Eq. 1 integrates the fast changes in the distribution of ice and open water areas resulting mainly from wind variability, which are difficult to measure otherwise. Furthermore, Pease (1987) found that the time required to open 10-20 km wide polynyas is generally between half a day and four days while the timescale in Eq. 1a is $t_2 - t_1 = 60$ days. This slow dynamics can be justified in part by the large size of western FB's polynyas (see Table III.2).

polynya	fetch (km)	A_{\max} (km ²)	\bar{z} (m)
Hall Beach (HaB)	32	560	15
along Melville Peninsula (MP)	7	620	36
Lyon Inlet (LI)	70	780	120

Table III.2. Main characteristics of western Foxe Basin's polynyas. The fetch and A_{\max} are the downwind width and the surface area of the fully open polynya, respectively, and \bar{z} is the mean depth under A_{\max} .

III.3. RESULTS

III.3.1. Heat fluxes calculations in western Foxe Basin's polynyas

III.3.1.1. Calculation for the 2003-2004 winter

Since the polynyas at HaB, MP and LI are all three located above the Arctic Polar Circle, the shortwave radiation contribution to the heat flux balance is negligible during the winter months. Typically, the net longwave and shortwave fluxes over the northern half of FB are approximately 210 and 17 Wm⁻² when averaged from December 20 to March 20, respectively, and around 240 and 150 Wm⁻² when averaged from March 20 to June 20. These values have been obtained from the numerical model of Saucier *et al.* (2004a); note that the model is not used here for the flux calculations above the polynyas because its horizontal grid resolution (10 km × 10 km) is of the same order as their sizes (see Table III.2). The longwave flux H_{LW} can be decomposed into the upwards and downwards contributions:

$$\begin{cases} H_{LW} = H_{LWup} - H_{LWdown} \\ H_{LWup} = \varepsilon_{sea} \sigma T_s^4 \\ H_{LWdown} = \varepsilon_{air} \sigma T_{10}^4 \end{cases} \quad (2a-c)$$

where $\varepsilon_{sea} = 0.98$ and ε_{air} are the emissivity of the water surface and of the atmosphere, so

that $\varepsilon_{air} = \int_{cc=0}^{cc=1} 0.729 (1 + 0.32 c^{2.75}) dc \approx 0.79$ is the mean value for a cloud cover (cc) fraction

varying from 0 to 1 of Hanesiak *et al.* (2001) recommended formulation (derived from

Maykut and Church, 1973), $T_s = -1.85$ °C is the water temperature in the polynya corresponding to the freezing point at the sea surface, T_{10} is the atmospheric temperature measured at 10 m height, and $\sigma = 5.67 \times 10^{-8}$ W m⁻² K⁻⁴ is the Stefan-Boltzmann constant. Not taking into account the shortwave radiation leads to a bias that becomes non-negligible as from the beginning of April until the end of May; in that case, the net heat flux is overestimated by more than 20 % (the reference flux being calculated by using the above value of 150 Wm⁻² for the shortwave contribution). In order to correct this bias, H_{LWup} is forced to cancel the contribution of H_{LWdown} at the end of the ice production period in FB's polynyas. With this constraint, which reduces the overestimation to around 10 %, Eq. 2b becomes:

$$\begin{cases} H_{LWup}(t_0 \leq t \leq t_1) = 301.25 \text{ Wm}^{-2} (\equiv \varepsilon_{sea} \sigma T_s^4) \\ H_{LWup}(t_1 < t \leq t_2) = \\ \quad H_{LWup}(t_1) - \frac{(t - t_1)}{(t_2 - t_1)} [H_{LWup}(t_1) - H_{LWdown}(t_2)] \end{cases} \quad (2b'-b'')$$

with t_0 = January 1 (when polynyas start to produce ice), t_1 = April 1 (when the shortwave radiations become non-negligible) and t_2 = May 31 (when the ice production period ends).

With the above simplification, the net heat flux H_{net} exchanged at the sea-atmosphere interface is:

$$H_{net} = H_S + H_L + H_{LWup} - H_{LWdown} \quad (3)$$

where H_S and H_L are the sensible and latent heat fluxes, respectively, which can be expressed as follow:

$$H_S = \rho_{air} C_p C_{H10} W_{10} (T_s - T_{10}) \quad (4)$$

$$H_L = L_v C_{E10} W_{10} (Q_s - Q_{10}) \quad (5)$$

In both Eq. 4 and 5, W_{10} is the wind speed component pushing the ice offshore and all subscripts "10" refer to values either measured or calculated at 10 m height. In Eq. 4, $\rho_{air} = 1.284 \text{ kg m}^{-3}$ is the air density, $C_p = 1.005 \times 10^3 \text{ J kg}^{-1} \text{ K}^{-1}$ is the specific heat of air at constant pressure and C_{H10} is the bulk transfer coefficient for sensible heat. In Eq. 5, $L_v = 25.04 \times 10^5 \text{ J kg}^{-1}$ is the latent heat of vaporization of water, C_{E10} is the bulk transfer coefficient for latent heat, $Q_s = 4.215 \times 10^{-3} \text{ kg m}^{-3}$ is the vapor density at the sea surface, and Q_{10} is the atmospheric vapor density. The parameters C_{H10} , C_{E10} and Q_{10} are calculated from Andreas and Murphy's (1986) formulations; note that the latter involves $C_{E10} = C_{H10}$. Furthermore, the weather data (W_{10} , T_{10} , and derived parameters) of HaB's station have been associated with HaB's polynya, and the data of RB's station both with LI's polynya and the polynya along MP for the calculation of the heat fluxes.

The heat loss at the polynya-atmosphere interface is then the product of the net heat flux H_{net} with the surface area $A(t)$. Here, the product $H_{net} \times A(t)$ is integrated over each day in order to obtain the value (in Joules) of the heat exchanged between the sea-surface and the atmosphere. This net daily surface heat exchange H_{sch} is written as:

$$H_{sch} = \int_{day} H_{net} \times A(t) dt \quad (6)$$

A positive value of H_{sch} represents a heat loss from the sea to the atmosphere. The results are shown in Fig. III.5 where peaks of heat exchange occurring in mid-February are clearly visible for LI and MP's polynyas. These peaks reach $46 \times 10^{15} \text{ J}$ at LI and $36 \times 10^{15} \text{ J}$ at MP while the mean between January 1 and May 31, *i.e.* the ice production period, is

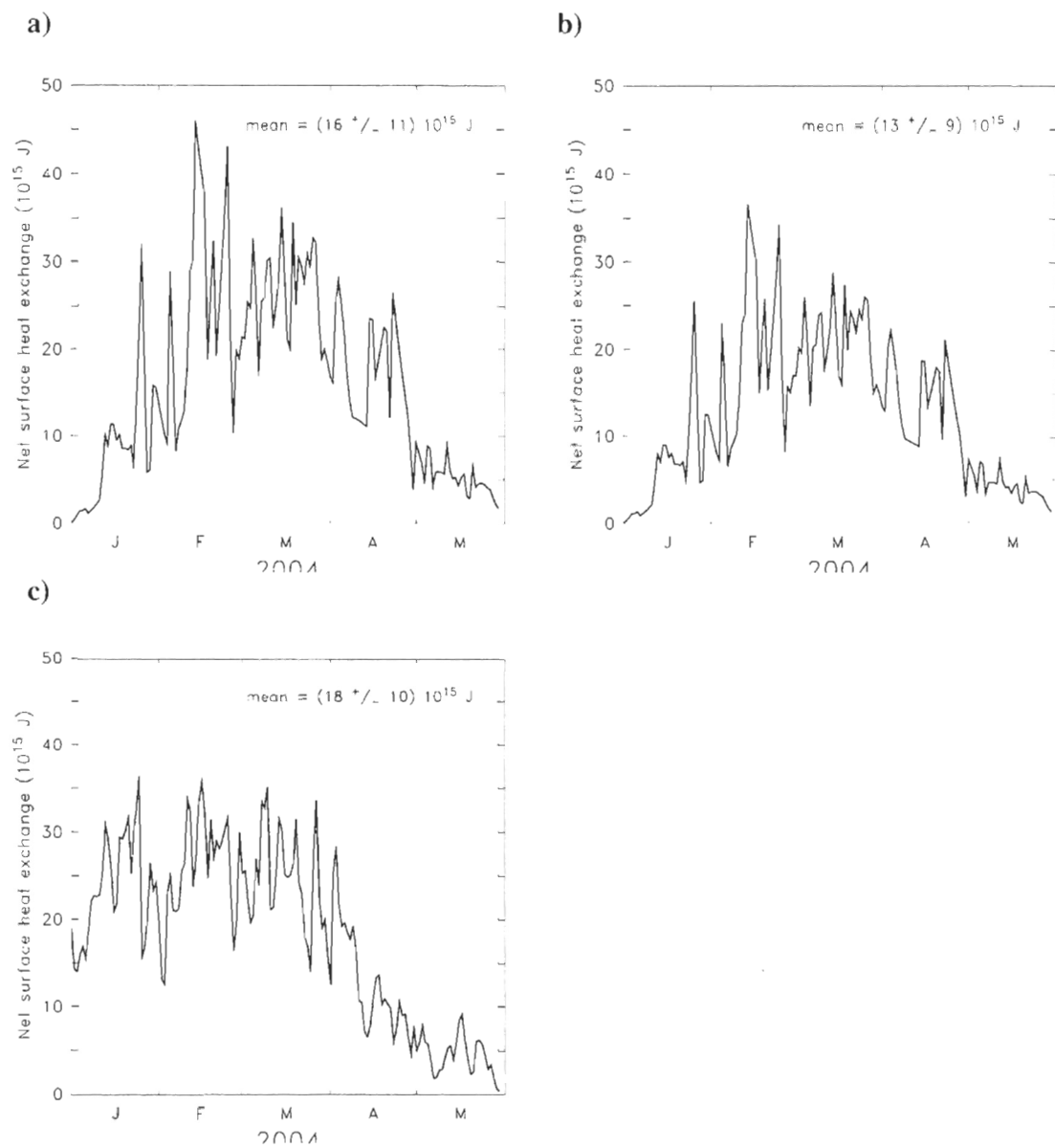


Fig. III.5. Net daily integrated sea-atmosphere heat exchanges in western Foxe Basin's polynyas. **a** corresponds to Lyon Inlet's polynya, **b** to the polynya along Melville Peninsula's eastern coast, and **c** to Hall Beach's polynya.

$(16 \pm 11) \times 10^{15}$ J at LI and $(13 \pm 9) \times 10^{15}$ J at MP. The curve at HaB's polynya is flatter: the maximal value reaching 36×10^{15} J while the mean is $(18 \pm 10) \times 10^{15}$ J.

It is also interesting to estimate the importance of each component in Eq. 3 by comparing their relative contributions from January 1 to May 31. The calculations are reported in Table III.3 where it is clear that the sensible heat is the main contributor ($\geq 60\%$) to the heat exchanges occurring at the surface of the polynyas. Note that, in Table III.3, the longwave contributions are given individually in order to show that the upwards flux is greater than the downwards flux, but it is the difference $H_{LWup} - H_{LWdown}$ which is used for the comparison with the other fluxes so that the sum of all relative contributions makes 100%. Also, these results tend to show that the sensible heat contribution increases as the air temperature gets colder (65% vs. 60%), *i.e.*, as the polynya is located further north.

III.3.1.2. Calculation for the years 1984-2006

The methodology used in Section III.3.1.1 for the 2003-2004 winter has been applied to the climatology. In particular, the same open water surface area function $A(t)$ (Eq. 1) has been used since it is known that polynyas occur at predictable locations (Muench, 1990); in western FB, they are either partially enclosed into MP (HaB and LI polynyas) or wedged against MP's eastern coast and Winter Island (the polynya along MP). The topography determines therefore both the location and shape of western FB's polynyas. Furthermore, here the slow polynya dynamics defined by Eq. 1 includes the interannual variability. The drawback of this method is that the effect of the mid-winter winds, already

polynya	\bar{H}_{net} [\bar{H}_{net}] (10^{15} J)	H_S^* [\bar{H}_S] (%)	H_L^* [\bar{H}_L] (%)	H_{LWup}^* [\bar{H}_{LWup}] (%)	H_{LWdown}^* [\bar{H}_{LWdown}] (%)	$H_{LWup}^* - H_{LWdown}^*$ [$\bar{H}_{LWup} - \bar{H}_{LWdown}$] (%)
Hall Beach (HaB)	18.2 [17.4]	65 [65]	4 [4]	77 [80]	46 [49]	31 [31]
along Melville Peninsula (MP)	12.8 [12.2]	60 [60]	5 [4]	95 [101]	60 [65]	35 [36]
Lyon Inlet (LI)	16.1 [15.4]	60 [60]	5 [4]	95 [101]	60 [65]	35 [36]
total:	47.1 [45.0]					

Table III.3. Relative contribution of the sensible H_S^* and latent H_L^* heats, and of the upwards H_{LWup}^* and downwards H_{LWdown}^* longwaves to the net heat exchanged at the polynyas' surface. In this table, all values of components are multiplied by each polynya's surface area and daily integrated. The asterisks indicate a value relative to \bar{H}_{net} , which is averaged from January 1 to May 31, and values between brackets have been averaged from 1984 to 2006.

smoothed by the climatology, is even more attenuated by the surface dynamics, resulting in a possible underestimation of the heat fluxes especially just after the polynyas opening. In order to evaluate this bias, a test has been performed using a modified version of Eq. 1a, considering the polynyas fully open as from February 1 instead of March 1; with this faster dynamics, the net heat flux is increased by almost 18 %. The results of the calculation with Eq. 1a left unmodified are shown in Fig. III.6. For the polynyas at LI and along MP, the peaks in heat flux are still visible in mid-winter although there are greater peaks at the beginning of March. For LI's polynya, the value of these peaks in February and March are equal to 27×10^{15} J and 33×10^{15} J, respectively, while the daily mean value is $(15 \pm 9) \times 10^{15}$ J between the beginning and the end of the ice production period (January 1 to May 31). For MP's polynya and for the same periods, the peaks are: 22×10^{15} J and 27×10^{15} J, respectively, while the mean is $(12 \pm 7) \times 10^{15}$ J. For HaB's polynya, the maximal value reaches 27×10^{15} J while the mean is $(17 \pm 8) \times 10^{15}$ J. It can be seen that for all polynyas, the mean heat flux exchanges are comparable to the ones obtained for the 2003-2004 winter; this is also true for each component in Eq. 3 (Table III.3). This is due to the similarity between the 2004 data in Fig. III.2b, c and the climatology in Fig. III.3. Since the air temperature and the wind speed are the two most important parameters governing the life cycle of latent heat polynyas, this also means that the 2003-2004 winter is representative and can be taken as reference for the thermodynamic processes occurring at the polynyas' surface. However, large SD values in Fig. III.3 indicate that the atmospheric variability over FB may exclude some years from the general pattern; the consequences may be important if this leads to a desynchronization between temperature minima and

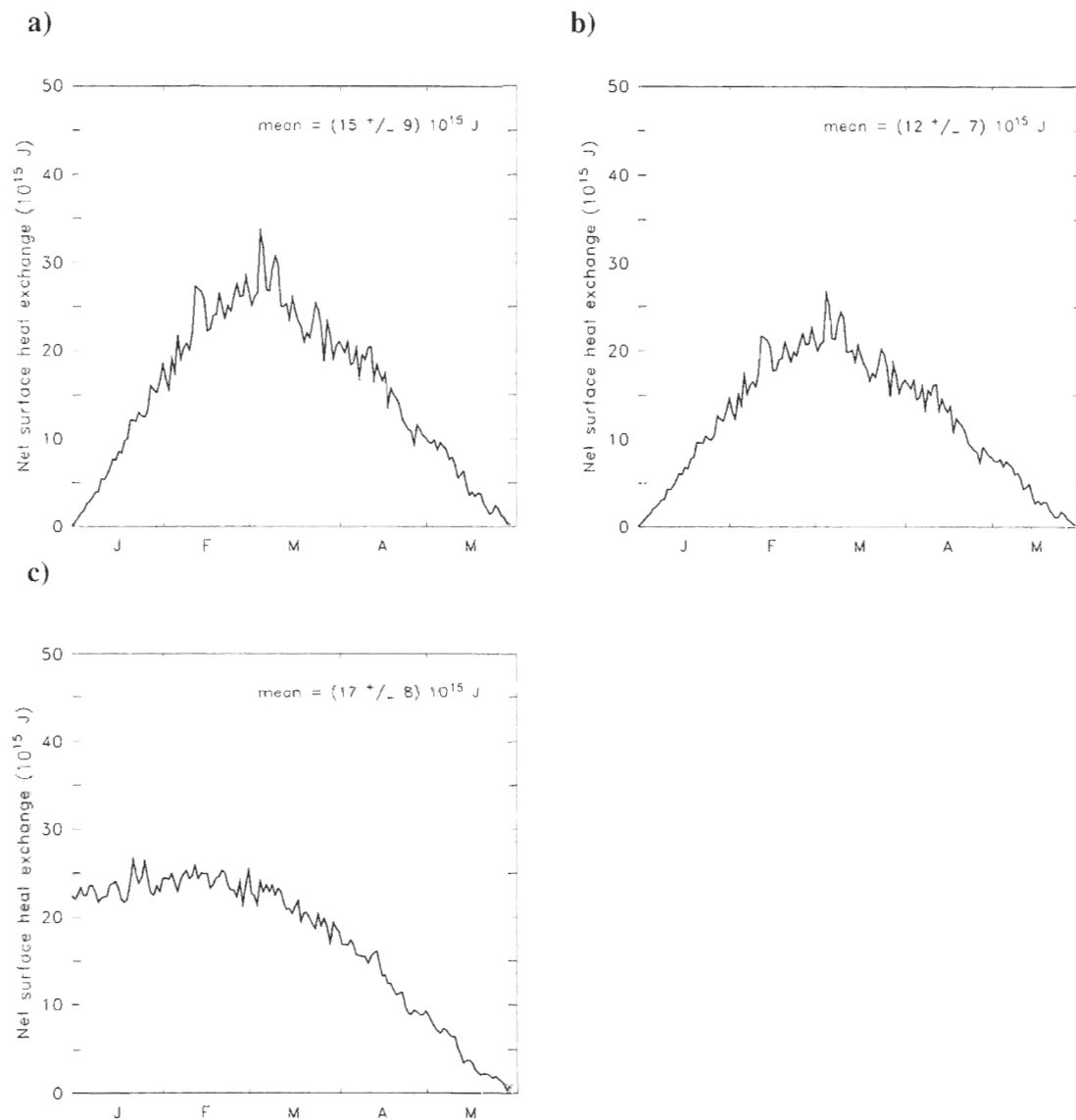


Fig. III.6. Sea-atmosphere heat exchanges averaged from 1984 to 2006 in Lyon Inlet's polynya (a), in the polynya along Melville Peninsula's eastern coast (b), and in Hall Beach's polynya (c).

wind maxima.

Note in Fig. III.5c and III.6c that the beginning of the curves is truncated in order to coincide with Figs. III.5a, b and III.6a, b time axes. This may underestimate the dense water production in HaB's polynya. However, when LI and especially MP's polynyas have not yet opened, the wind-driven circulation toward FC is impeded by the presence of sea-ice. The dense waters formed in HaB are likely to remain in the area where they can mix with the lighter waters coming from Fury and Hecla Strait, although some may begin to spread in the shallow channel along MP. This is difficult to quantify, but since the air temperature in November-December is not minimal and the projected wind not maximal, the effective amount of dense water produced during this period is probably not very large.

III.3.2. Production of dense water in western Foxe Basin's polynyas

III.3.2.1. Calculation of the produced sea-ice and rejected salt masses

Knowing the amount of heat loss from the sea to the atmosphere, it is then possible to calculate the mass M_{ice} of sea-ice produced through the polynyas. This is done by integrating the net daily heat exchanged during the period when the polynyas are active from $t_1 = \text{January 1}$ to $t_2 = \text{May 31, 2004}$ and by dividing the result by the latent heat of fusion for sea water ($L = 335.51 \times 10^3 \text{ J kg}^{-1}$), *i.e.*:

$$M_{ice} = \frac{1}{L} \sum_{t_1}^{t_2} H_{srh} \quad (7)$$

This calculation shows that LI, MP and HaB's polynyas have produced a total of 21.2×10^{12} kg of sea-ice in 2004 (Table III.4).

polynya	M_{ice} [\bar{M}_{ice}] (10^{12} kg)	M_{salt} [\bar{M}_{salt}] (10^{12} kg)	V_{dw} [\bar{V}_{dw}] (10^{12} m ³)
Hall Beach (HaB)	8.2 [7.8]	0.20 [0.19]	0.59 [0.56]
along Melville Peninsula (MP)	5.8 [5.5]	0.14 [0.14]	0.42 [0.40]
Lyon Inlet (LI)	7.3 [7.0]	0.18 [0.17]	0.52 [0.50]
total:	21.2 [20.2]	0.53 [0.50]	1.53 [1.46]

Table III.4. Calculation of sea-ice mass (M_{ice}), rejected salt mass (M_{salt}) and dense water volume (V_{dw}) produced in western Foxe Basin's polynyas during the 2003-2004 winter. Values between brackets have been averaged from 1984 to 2006.

From M_{ice} , one can readily estimate the total rejected salt mass M_{salt} through the polynyas:

$$M_{salt} = (S_s - S_i) \cdot 10^{-3} \times M_{ice} \quad (8)$$

where S_s is the mean surface salinity and S_i the mean salinity of the sea-ice. According to Prinsenbergh (1986), the observed surface salinity in FB is between 29 and 33.2, although large variations occur due to the melting of ice floes and river runoff. The mean surface salinity at western FB's polynyas averaged from t_1 to t_2 (defined above) for the years 2002 to 2005 varies between 31.6 and 33.1 (results obtained from the numerical model of Saucier *et al.*, 2004a). So, a mean value of $S_s = 32.4$ is chosen here for the calculation of M_{salt} . Furthermore, Shokr and Barber (1994) found that the mean salinity for the first year sea-ice in Resolute Passage (Canadian Eastern Arctic) is 7.5; here, due to the proximity of this area with FB, S_i is taken equal to this value. Note, however, that $S_i = 7.5$ is a minimum since the salinity of frazil ice is likely higher, but variable and difficult to evaluate. With these assumptions, Eq. 8 gives for the 2003-2004 winter an estimated amount of total rejected salt in the polynyas of 0.53×10^{12} kg (Table III.4). Given the uncertainty on the surface salinity value, the total mass of salt lies between 0.51×10^{12} ($S_s = 31.6$) and 0.54×10^{12} kg ($S_s = 33.1$).

The same methodology has been applied with the climatology, using the net heat fluxes of Table III.3. The results obtained for the sea-ice and rejected salt mass are: $M_{ice} = 20.2 \times 10^{12}$ kg and $M_{salt} = 0.50 \times 10^{12}$ kg (Table III.4). It can be seen that they are very close to those found for 2004.

It is useful to compare the amount of ice produced in the polynyas with the total

estimated mass of ice formed in FB during the winter. Two methods are used here in order to calculate this mass: 1) Saucier *et al.* (2004a) numerical model for the year 2004; and 2) Lebedev's (1938, in Bilello, 1961) empirical formula, based on observations of sea-ice accretion made in Russian Arctic seas, for the 1984-2006 period. While the numerical model gives a good estimate of the amount of ice produced in the whole basin, because its results are reliable at the mesoscale, the value obtained from the empirical formula should be regarded as an underestimation since it does not take into account the percentage of ice leaving the basin, estimated at 31 % by the model.

With the numerical model, the integration of the ice growth rate over FB shows that a volume of ice of around $0.45 \times 10^{12} \text{ m}^3$ has been produced in 2004. Multiplying this volume by the ice density ($\rho_{ice} = 917 \text{ kg m}^{-3}$) gives a total mass of $4.1 \times 10^{14} \text{ kg}$.

With Lebedev's formula, which expresses the ice thickness e (in meter) as a function of the cumulative freezing degree days (FDD) over the basin, so that:

$$e = 1.33 \times 10^{-2} \times FDD^{0.58} \quad (9)$$

the volume of ice can be calculated by multiplying e with the surface area of FB ($0.2 \times 10^{12} \text{ m}^2$, Table III.1). Fig. III.3a, b shows that, on average, the air temperature T_{10} in FB is below the freezing sea surface temperature T_s from $t_1 = \text{September 28}$ to $t_2 = \text{May 29}$

(of the following year), thus $FDD = 1 \text{ day} \times \sum_{t_1}^{t_2} (T_s - T_{10}) \approx 4558 \text{ }^\circ\text{C day}$ and $e \approx 1.8 \text{ m}$. The

volume of ice produced, estimated with the climatology, is then $0.35 \times 10^{12} \text{ m}^3$, which represents a total mass of around $3.2 \times 10^{14} \text{ kg}$.

The contribution of FB's western polynyas accounts therefore for 5 %

($21.2 \times 10^{12} / 4.1 \times 10^{14}$) to 6 % ($20.2 \times 10^{12} / 3.2 \times 10^{14}$) of all the ice produced in the basin while their combined surface area is only $1960 \times 10^6 \text{ m}^2$, *i.e.*, less than 1 % ($1960 \times 10^6 / 0.2 \times 10^{12}$) of FB's whole surface. In other words, the production rate of sea-ice is five to six times higher in the coastal polynyas than in the rest of the basin.

III.3.2.2. Calculation of the dense water volume

Defossez *et al.* (2008) have shown that the deep water in FC is the result of the mixing of two distinct water masses: the previous year's deep waters with the newly formed dense waters coming from western FB's polynyas. The latter form a dense water tongue reaching 140 m height which affects the water column as it flows southeastwards at depth in the channel. To simplify the calculations, it is assumed here that, in winter: 1) FB is a system of only two water masses constituted of the dense water gravity current flowing inside surrounding waters having the deep water characteristics; and 2) when a large amount of dense water forms rapidly at the polynyas' surface, it sinks immediately without being mixed by the surrounding water. The first assumption is true at depth and still reasonable near the surface since the autumn storms preceding the sea-ice and dense water formation tend to homogenize the water column in FB. The second assumption is also justified since, during the pulse, the dense water temperature measured at 440 m depth corresponds to the freezing point at the sea-surface and has therefore not been altered during its travel from the polynyas to the bottom of FC. It follows from these assumptions that, when a fraction of volume V_{fsw} of surrounding water taken at the polynyas' surface freezes, it produces sea-ice and a corresponding volume V_{dw} of dense water. This process is summarized in Fig. III.7.

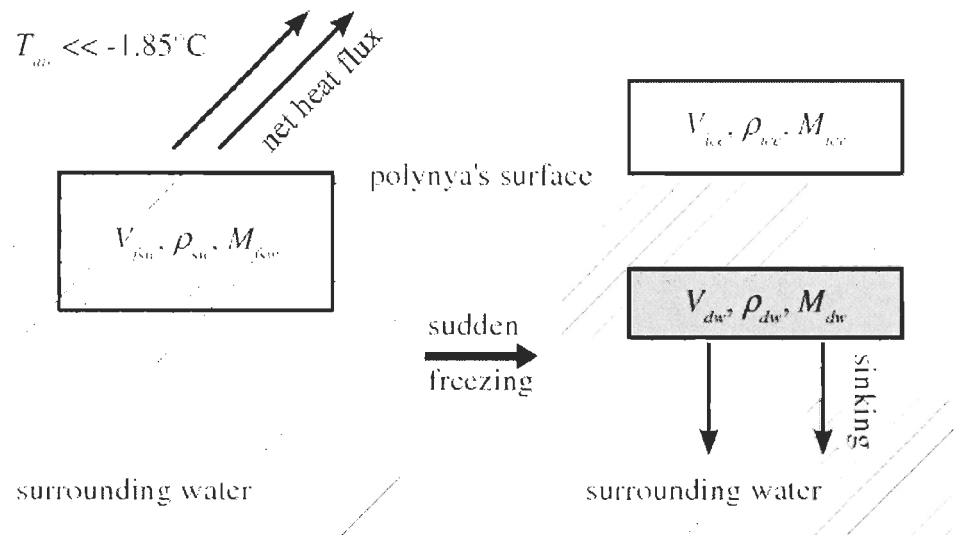


Fig. III.7. Schematic representation of frazil ice and dense water formation following intense heat loss at a latent heat polynya's surface. (see text for the parameters' definitions)

So, conservation of mass and volume leads to a system of two equations with two unknowns :

$$\begin{cases} \rho_{sw} V_{fsw} \approx \rho_{dw} V_{dw} + M_{ice} \text{ (mass conservation)} \\ V_{fsw} \approx V_{dw} + \frac{M_{ice}}{\rho_0} \text{ (volume conservation)} \end{cases} \quad (10\text{a-b})$$

where ρ_{sw} and ρ_{dw} are the densities of the surrounding and dense waters, respectively, and $\rho_0 = 1000 \text{ kg m}^{-3}$ is the fresh water density. In Eq. 10, note that the mass of salt and brine pockets trapped in the ice is neglected, as well as the expansion due to the small differences in temperature and salinity between the surrounding and dense waters. Note also that $\frac{M_{ice}}{\rho_0}$ corresponds to a fresh water volume, *i.e.*, the volume of water resulting from the melting of an amount M_{ice} of ice. Only V_{dw} is of interest here. So, by substituting V_{fsw} in Eq. 10, V_{dw} can be written as a function of the mass of ice produced by the polynyas:

$$V_{dw} \approx \frac{\rho_{sw} - \rho_0}{\rho_{dw} - \rho_{sw}} \times \frac{M_{ice}}{\rho_0} \quad (11)$$

The characteristics of the dense water produced in FB can be obtained from Fig. III.2a by taking the minimum of temperature and maximum of salinity during the pulse measured at 440 m, *i.e.*: $T_{dw} = -1.85 \text{ }^\circ\text{C}$ ($= T_s$) and $S_{dw} = 33.75$ and therefore $\rho_{dw} = 1029.28 \text{ kg m}^{-3}$. Fig. III.2a also provides the characteristics of the surrounding waters at the bottom of FC: $T_{sw} = -1.64 \text{ }^\circ\text{C}$, $S_{sw} = 33.27$ and $\rho_{sw} = 1028.88 \text{ kg m}^{-3}$. Given these values, Eq. 11 gives an amount of $1.53 \times 10^{12} \text{ m}^3$ of dense water produced by the three polynyas during the year 2004. The calculations for each polynya is summed up in

Table III.4. Since FB's volume is $18.0 \times 10^{12} \text{ m}^3$ (Table III.1), the renewal of the deep water in FC corresponds to 8.5 % ($1.53 \times 10^{12} / 18.0 \times 10^{12}$) of the entire basin.

The same methodology has been applied with the climatology, using the same surrounding and dense water characteristics as in 2004. In this case, $1.46 \times 10^{12} \text{ m}^3$ of dense water have been produced by the polynyas (Table III.4). The comparison between the 2003-2004 winter and the climatology shows very similar results. This reinforces the hypothesis suggested in Section III.3.1.2 that 2004 is a typical year which can be used as reference, from the viewpoint of atmospheric conditions, when studying FB's dense water production in winter.

It is interesting to compare the volume of the incoming dense water mass with the deep water volume in FC. The latter is difficult to estimate because its distribution varies with time and is uneven in the channel. However, since the deepest trough in FC is at 450 m depth and the maximal height of the dense water mass is 140 m, the volume under the mid-depth of the channel is a clear overestimation of the deep water volume, *i.e.*, the volume deeper than 220 m is greater than the volume under 310 m (450 - 140). Therefore, the volume of dense water produced in the polynyas ($1.53 \times 10^{12} \text{ m}^3$) exceeds the deep waters' prism ($1.4 \times 10^{12} \text{ m}^3$, Table III.1). This means that the dense water pulse not only has the capacity to renew most of FC's deep waters but can also partially leave FB and overflow into the other parts of the HB system.

III.4. DISCUSSION

III.4.1. Dense water production in western Foxe Basin's polynyas

Strong winter winds lead to the opening of Arctic coastal polynyas where large sea-atmosphere heat fluxes take place due to the exposure of open water to very low air temperatures (Andreas and Murphy, 1986; Smith *et al.*, 1990; Chapman, 1999). Fig. III.2b, c and Fig. III.3 show that these conditions are met in western FB during winter. Three large polynyas at LI, along MP and at HaB lose daily, in average, a total of $(16.1 + 12.8 + 18.2) \times 10^{15} = 47.1 \times 10^{15}$ J of heat (Table III.3) to the atmosphere between January 1 and May 31, 2004. This, in turn, produces dense waters which eventually flow into FC with a mean annual transport of around 0.05 Sv (1.53×10^{12} m³ for one year, Table III.4). This value is not negligible compared to the mean annual brine flux, comprised between 0.7 and 1.2 Sv, produced by the coastal polynyas of the entire Arctic (Cavalieri and Martin, 1994). Note that Cavalieri and Martin chose a reference salinity of 32.85 for the brine which is less than the observed salinity of 33.75 at the bottom of FC during the pulse. The climatology gives similar results with a total heat loss, for the three polynyas in FB, of $(15.4 + 12.2 + 17.4) \times 10^{15} = 45.0 \times 10^{15}$ J (Table III.3) and a dense water transport of approximately 0.05 Sv (1.46×10^{12} m³ per year, Table III.4)

If the calculation of the dense water transport is made over the actual period of dense water production, *i.e.* from January 1 to May 31, instead of one year, then the mean transport becomes 0.12 Sv for 2004 and 0.11 Sv with the climatology. This value is three

times higher than the estimated transport (0.04 Sv; Sadler, 1982) in winter through Fury and Hecla Strait. This makes the dense water pulse the main current component in FB during the winter months and therefore an important contributor to the general circulation in the basin.

It is also useful to estimate the speed of the gravity current in FC. Since the bottom of the channel slopes down steadily from LI (120 m mean depth) to the mooring (440 m) 140 km further with no topographical obstacle, the dense water mass can flow without hindrance. By assuming that the peak of northwesterly winds on January 25 (Fig. III.2b) marks approximately the opening of western FB's polynyas, and knowing that the dense water pulse is detected on April 5 (Fig. III.2a), the dense water mass travels southeastwards along the channel at a mean speed of $140 \times 10^3 \text{ m} / 71 \text{ days} \approx 2.3 \times 10^{-2} \text{ ms}^{-1}$. This value is in the range $1.7 \times 10^{-2} - 3.6 \times 10^{-2} \text{ ms}^{-1}$ found by Defossez *et al.* (2008) with a method based on differences in densities between the surrounding and dense water masses.

Lastly, the gravity current speed provides another means to estimate the dense water volume since the height of the incoming dense water mass is known as well as the cross section passing through the mooring's location in FC's deepest trough. This can be written as:

$$V_{dw} \approx v_{dw} A_{cs} \Delta t \quad (12)$$

where v_{dw} is the speed of the dense water mass, $A_{cs} = 4.9 \times 10^6 \text{ m}^2$ (calculated from ETOPO2, NOAA) is the cross sectional area from (64.3 °N, 81.5 °W) to (65.8 °N, 81.3 W) and comprised between the bottom of the channel (maximum depth at 450 m) and the top of the dense water tongue (which is at $450 - 140 = 310 \text{ m}$ depth), and Δt is the duration of

the dense water pulse (from April 5 to June 30, 2004). The approximation in Eq. 12 is essentially due to the uncertainty of v_{dw} . With v_{dw} equal to 1.7×10^{-2} , 2.3×10^{-2} and $3.6 \times 10^{-2} \text{ ms}^{-1}$, Eq. 12 gives 0.63×10^{12} , 0.86×10^{12} and $1.34 \times 10^{12} \text{ m}^3$, respectively, which is less but still reasonably close to the more accurate result ($1.53 \times 10^{12} \text{ m}^3$) obtained with Eq. 11. This suggests that the actual value of the gravity current speed is likely closer to its upper limit, *i.e.* to $3.6 \times 10^{-2} \text{ ms}^{-1}$.

III.4.2. Consequences of the mid-winter opening of western Foxe Basin's polynyas

The previous results can be summarized chronologically in order to reconstruct the entire cycle of dense water production in FB: a) as soon as the beginning of winter, *i.e.* by the end of October when the whole basin starts to freeze because of air temperatures below $-12 \text{ }^\circ\text{C}$, the winds create and maintain the polynya at HaB on FB's shallow shelf; b) from HaB's polynya, dense waters are produced and begin to flow along the eastern coast of MP towards FC; c) strong winds, and especially their northwesterly component with peaks close to 20 ms^{-1} , occur in mid-winter when the air temperature is minimal over FB (less than $-30 \text{ }^\circ\text{C}$ in January-February) and open simultaneously the polynyas at LI and along MP. Note that although RB's polynya opens at the same time as can be seen in Fig. III.4b, it is not taken into account in this study because a sill at 70 m as well as the mean circulation prevent dense waters produced there from flowing into FC. For similar reasons, the polynyas located north of HaB are neglected here since it is unlikely that dense water form in the vicinity of Fury and Hecla Strait (because of significant mixing and freshwater input from two rivers and the strait) and that sills at 30-40 m would prevent it to flow

southwards; d) still in mid-winter, the dense waters coming from HaB merge with those produced along MP's polynyas and add up with the deep convection taking place in LI's polynya, thus creating a pulse of dense water which propagates along FC; and e) this gravity current mixes and replaces most of the deep waters at depth in FC, and partially overflows into HB in summer, because of the time needed to travel the length of FC, which ends the cycle for the considered winter. The dense water pulse observed in FC can therefore be described as the sum of two distinct phenomena, a cascade of dense water coming from HaB by skirting along MP towards FC and deep convection inside LI, both synchronized when southwestern FB's polynyas open in mid-winter.

According to Ivanov *et al.* (2004), the life cycle of gravity currents such as dense water cascades can be divided into four phases: pre-conditioning, active, main and final stages. This classification applies well for the dense waters coming from HaB and cascading into FC as shown in the following paragraphs.

During the pre-conditioning stage, the dense waters produced at HaB tend to accumulate on northern FB's shallow shelf. This accumulation may be due not only to the slight bathymetric rebound before the topographic break in the vicinity of Winter Island but also, according to Carmack and Chapman (2003), to an ice edge relative to the underlying topography which is likely to form at shelf breaks where density fronts appear.

The start of the active stage is well defined in time and corresponds to the opening of southwestern FB's polynyas. When the ice cover is displaced seaward, which in Fig. III.4b results in some ridging subsequent to the convergence and compression of ice along MP's eastern coast, the frictional effect due to the ice is removed and the dense

waters accumulated in the shallow channel along MP can flow freely into FC. The ice cover and ice edge near Winter Island play therefore the role of a valve for the gravity current in FB. This "tap" effect may be important in the Arctic since, when polynyas open up in mid-winter, they may alter the halocline over great distances by producing energetic dense water currents. As polynyas are common in polar regions, it is likely that this effect is not unique to FB. An example of a potential candidate could be the North Water polynya north of Baffin Bay which, according to Smith *et al.* (1990), is not continually present in winter but occurs in a pulsewise fashion.

The effect of the main stage is visible in Fig. III.2a where, for a period of around three months corresponding to the pulse, the dense water properties remain almost constant. Lastly, the detection of the dense water mass at the mooring's location shows that the cascading waters have spread off the topographic break near Winter Island and that they have followed FC's bathymetry, thus entering the final stage. Note, however, that the classification of Ivanov *et al.* must be amended in the case of FB's cascade because the active and main stages are strengthened by the deep convection occurring in LI's polynya. Indeed LI's contribution accounts for 34 % ($7.3 \times 10^{12} / 21.2 \times 10^{12}$, Table III.4) of all the dense waters produced in FB's western polynyas.

III.4.3. Atmospheric pressure and synoptic scale

In the previous sections, the discussion has concentrated on local events like the mid-winter opening of polynyas and the succession of phenomena that follow. In particular, this has been useful to explain the pulse-like propagation of the gravity current at the

bottom of FC. Typically, the scale of these phenomena ranges from a few tens of kilometers (the width of the polynyas) to a few hundreds of kilometers (the distance traveled by the dense water pulse); however, their recurrence implies that larger scale mechanisms are likely at work in FB. For example, Déry and Wood (2004) have shown that the river runoff variability in HB is strongly linked to the Arctic Oscillation (AO), which probably also impacts the freshwater balance of the whole HB system. The AO is characterized by the variations of the sea-level atmospheric pressure, relative to the mean winter sea-level pressure (SLP) north of the 20°N latitude, so that a positive (negative) AO index corresponds to a pressure below (above) the mean SLP at latitudes higher than 45°N and above (below) the mean SLP at latitudes comprised between 20°N and 37°N. The AO can also be regarded as the surface signature of the polar vortex strength and, as such, the general pattern of the wind field over FB may depend on the AO index (Thompson and Wallace, 1998). When the index is positive, northwesterly winds bring dryer and colder air from the Canadian Arctic, and, when it is negative, northeasterly winds bring wetter and warmer air from the Labrador Sea (Thompson and Wallace, 2001). Therefore, the dense water production in FB is likely to be greater during a positive phase of the AO, although the non-linear behavior of the ice formation in the polynyas may lead to unexpected results. Because of these possibly important implications, clues about synoptic scale driving forces in the basin, that set into motion the air and water masses during winter, are given here.

In order to advect cold air masses from the Arctic to the HB system, the meridional atmospheric pressure gradient must have a component directed northwards. It is therefore interesting to check, at least roughly, the orientation of this gradient in mid-winter by

comparing data obtained in northwestern FB (at HaB) and southeastern HB (at Kuujjuarapik). Fig. III.8a shows that the pressure at HaB markedly exceeds that at Kuujjuarapik for almost two months from January 15, 2004, whereas the inverse situation prevails for most of the year. This has a great impact on the wind pattern as drawn in Fig. III.9: in **a**, the velocity field averaged from January 1 to 16 shows weak winds with no dominant direction whereas, in **b**, the average from January 16 to 31 shows strong northwesterly winds. The latter are ideally oriented to open western FB's polynyas since they are almost perpendicular to MP's eastern coast.

However, the climatology in Fig. III.8b indicates that although the meridional inversion of pressure seems to be characteristic in the HB system, it generally occurs at the end of March, *i.e.*, too late to help opening the polynyas. This observation does not contradict the above conclusions because the climatology erases the pressure peaks, but it suggests that the state of the AO may affect the polynyas' dynamics, as well as the sea-atmosphere heat transfers and the dense water production in FB.

If the AO does indeed modulate the dense water production, it must consequently affect the sedimentation rate at the bottom of FC. This idea is illustrated in Fig. III.10 where a particle sinks more slowly and is carried away further in the channel when it enters the dense water mass. The strength of the gravity current can therefore filter the particles according to their density and their drag coefficient. This could provide a way to study the past climate by looking for the AO signature in FC's sediments. Note that FB is a system with sediment rich waters and ice, especially in the northeastern tidal flats, since strong tides and wind induced currents generate a lot of friction with the bottom of the basin. The

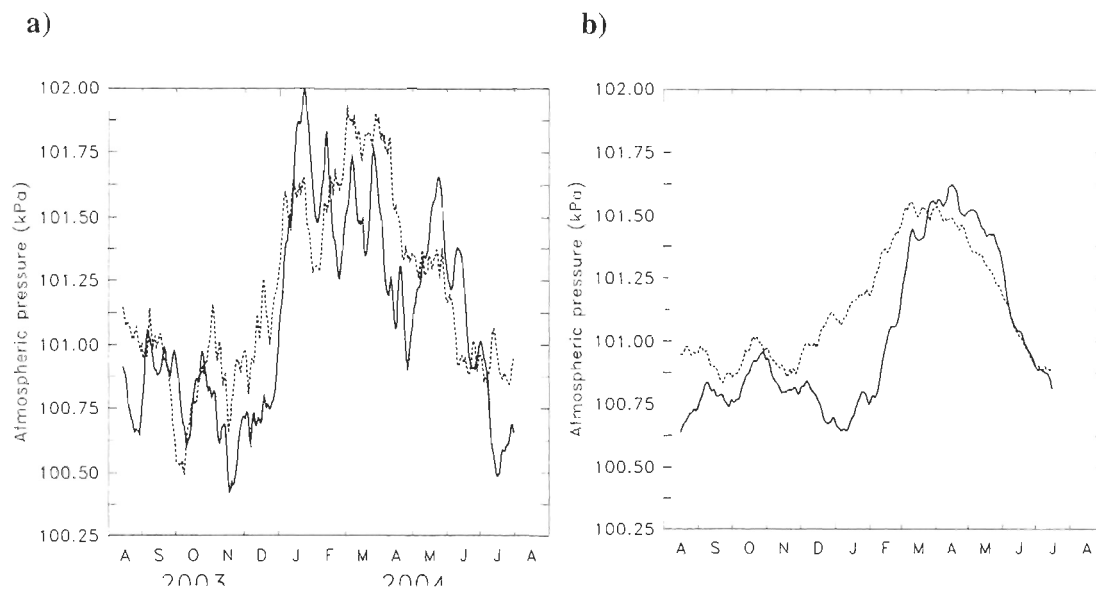


Fig. III.8. Comparison of surface air pressure in the north and south of the Hudson Bay system. The solid line represents the pressure at Hall Beach and the dashed line the pressure at Kuujuarapik. In **b**, the data have been averaged from 1984 to 2006.

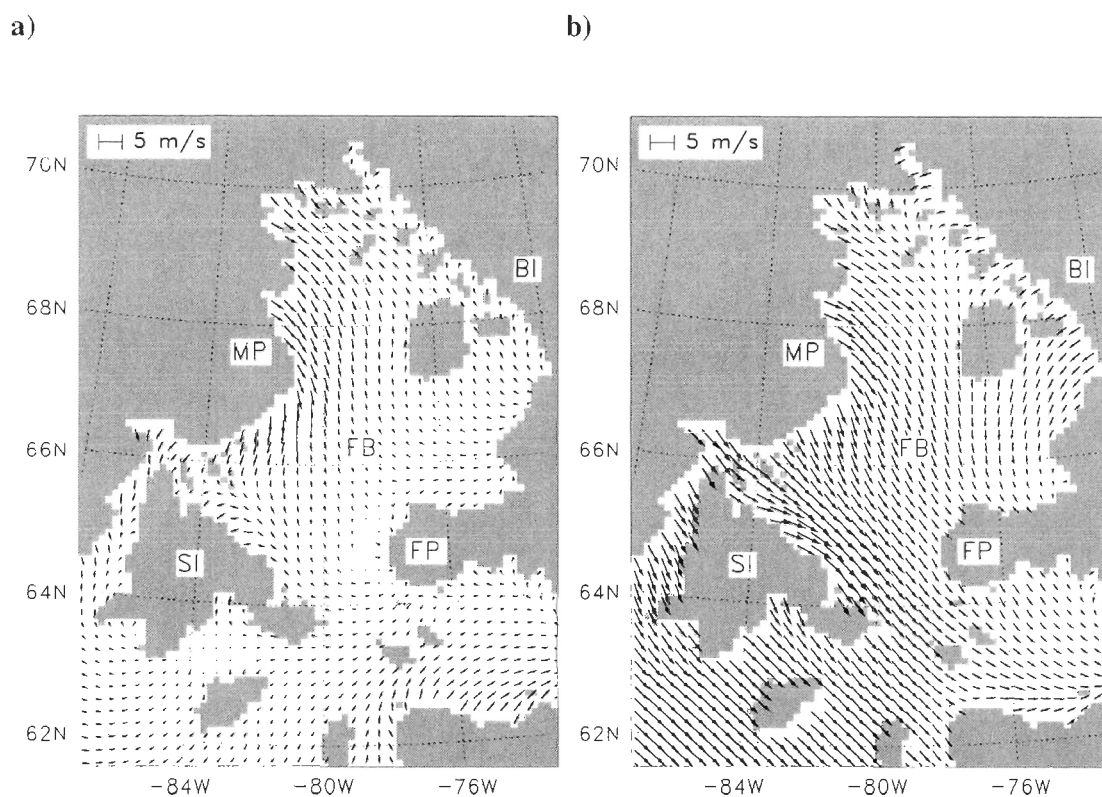


Fig. III.9. Consequence of the meridional inversion of the atmospheric pressure in mid-winter and over the Hudson Bay system on the wind velocity field at 10 m height in Foxe Basin. The data come from the Global Environmental Multiscale model (Canadian Meteorological Center). The vectors have been averaged from January 1 to 16, 2004, and from January 16 to 31, 2004, in **a** and **b**, respectively (see Fig. III.1 for acronyms signification).

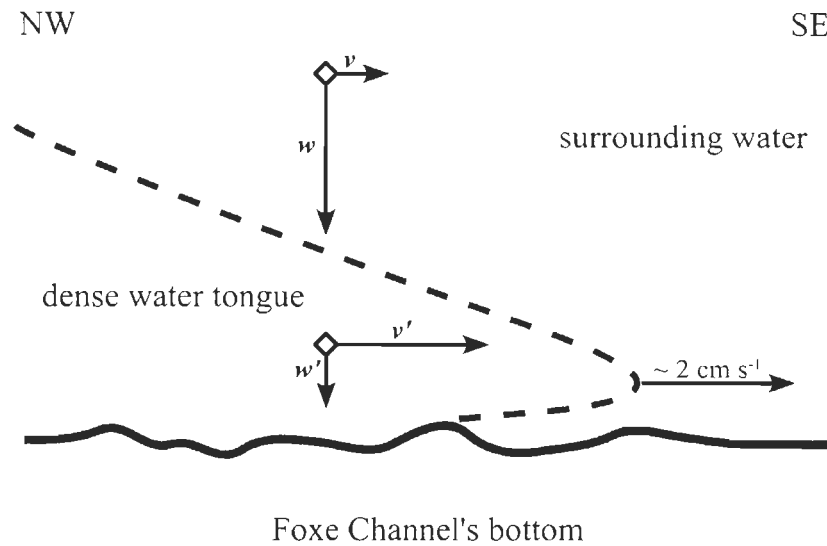


Fig. III.10. Schematic representation of the incoming dense water mass at the bottom of Foxe Channel in winter and of its effect on sedimentation. The dashed line represents the front separating the dense waters from the surrounding waters. The lozenges symbolize a particle. Its horizontal and vertical speed components are, respectively, v and w when it sinks in the surrounding waters, and become $v' > v$ and $w' < w$ when it enters the dense water mass. NW stands for northwest and SE for southeast.

system might even be prone to turbidity currents and, in that case, they should also be studied in order to assess their role in FB's oceanography.

III.5. CONCLUSION

This study has shown that western FB's polynyas play a major role in the deep water renewal in the basin due to large heat exchanges at the sea-atmosphere interface leading to the production of great amounts of brine rich cold waters. The dense waters coming from HaB by skirting along MP add up with the deep convection occurring in LI when FB's southwestern polynyas simultaneously open up in mid-winter. The combination of these two phenomena generates a dense water pulse which is detected at depth far from the production area. Bibliographical and climatological data give strong clues that this is a recurrent phenomenon, although there may be some variability depending on the AO index. The large amount of dense water produced in the polynyas is carried away by energetic currents. It replaces most of FC's deep waters by mixing with them and can probably overflow the sill at 180 m between Southampton Island and Nottingham Island, thus allowing FB's dense waters to enter HB.

FB's western polynyas also produce large amounts of sea-ice. The role of the ice in FB is complex because it not only isolates the sea from the atmosphere, thus effectively inhibiting heat and momentum fluxes, but it also acts as a valve at the shelf break which allows the synchronization of the cascade of dense water with the deep convection when LI's polynya opens up. Another complication arises from the variety of scales involved by the phenomena leading to the ice formation (for a detailed description of the different scales, see Gow and Tucker, 1990): molecular scale with ice crystals, millimetric scale with

frazil ice, centimetric to decametric scale with pancake and drifting ice, and mesoscale with the polynyas' dynamics. All this makes the analytical study of ice and dense water production in the polynyas as difficult as the study of turbulence, and the difficulty is increased by the lack of observations available from these regions.

By end of the 21st century and according to the Intergovernmental Panel on Climate Change (IPCC, 2007), the global surface warming is expected to be between 1.8 °C (scenario B1) and 3.4 °C (scenario A2). In arctic regions, the warming will be 1.5 to 4.5 times higher than the global prediction due to the polar amplification (Holland and Bitz, 2003). Since polynyas are very dependent on atmospheric temperatures and winds, it is likely that the dense water production in FB will be weakened. The consequences would be great on the general circulation not only in FB but also in the whole HB system because less dense waters would overflow into the bay. Furthermore, a lesser renewal of the deep waters would probably have an impact on the biology at the bottom of FC since the ventilation by cold and oxygen rich waters would be lessened. A systematic survey of Arctic polynyas could therefore provide useful climate records since the dense waters they produce contain information about the atmospheric events that created them.

**IV. COMPARING WINTER AND SUMMER ESTUARINE
CIRCULATION IN FOXE BASIN, CANADA**

ABSTRACT

Foxe Basin is an inland sea north of Hudson Bay, connected to the Arctic via the Gulf of Boothia and to the Labrador Sea via Hudson Strait. The basin is ice covered more than six months per year and exports one third of its ice toward the Labrador Sea. It is a place where, in winter, latent heat polynyas to the west coexist with sensible heat polynyas around southwestern Foxe Peninsula, the latter resulting from an upwelling of intermediate water. The sea-ice induces a phase advance of 7° to the main tidal constituent at mid-depth; it affects also the circulation by friction and by extracting freshwater from the sea surface. The salt balance versus depth at the outlet of Foxe Basin shows that the estuarine circulation forms a positive-negative couple in summer and winter; this may be used to evaluate the global warming impact in this Arctic-Subarctic region.

IV.1. INTRODUCTION

The oceanographic circulation in Foxe Basin (FB), a large and shallow estuarine inland sea north of the system of the Hudson Bay (HB, Fig. IV.1), exhibits quite different patterns in winter and summer. FB's main features are briefly described in this section. FB is bordered to the north and northeast by Baffin Island (BI), to the west by Melville Peninsula (MP) and to the south by Southampton Island (SI). The basin has a surface area of around $0.2 \times 10^{12} \text{ m}^2$ and a mean depth of 90 m (from ETOPO2, NOAA), it receives Arctic water through Fury and Hecla Strait (FHS) and is connected to the Labrador Sea (LS) via Hudson Strait (HS). Although the throughflow of Arctic water toward the North Atlantic via the HB system is small compared to the other fairways of the Canadian Arctic Archipelago, this region plays an important hydrographic role by exporting freshwater into the LS. Quantitatively: a) in winter, well mixed Arctic water flows through FHS at 0.04 Sv ($1 \text{ Sv} \equiv 10^6 \text{ m}^3 \text{ s}^{-1}$) with a salinity of $S = 32$ and a temperature of $T = -1.7 \text{ }^\circ\text{C}$ (Barber, 1965) while, in summer, the throughflow is at 0.1 Sv with $S = 31$ and $T = 0.8 \text{ }^\circ\text{C}$ (Sadler, 1982). By comparison, 2.0 Sv of seawater flow from the Baffin Bay to the LS through Davis Strait (annual estimate, Melling *et al.*, 2006); and b) 29×10^{-3} Sv of oceanic freshwater and 6×10^{-3} Sv of ice flow through HS (Saucier *et al.*, 2004a), while the corresponding estimated values through Davis Strait (Melling *et al.*, 2006) are 100×10^{-3} Sv of freshwater and 19×10^{-3} Sv of ice. According to Drinkwater (1988), the net flow out of HS into the LS should be approximately 0.1 Sv, which corresponds to the net flow through FHS

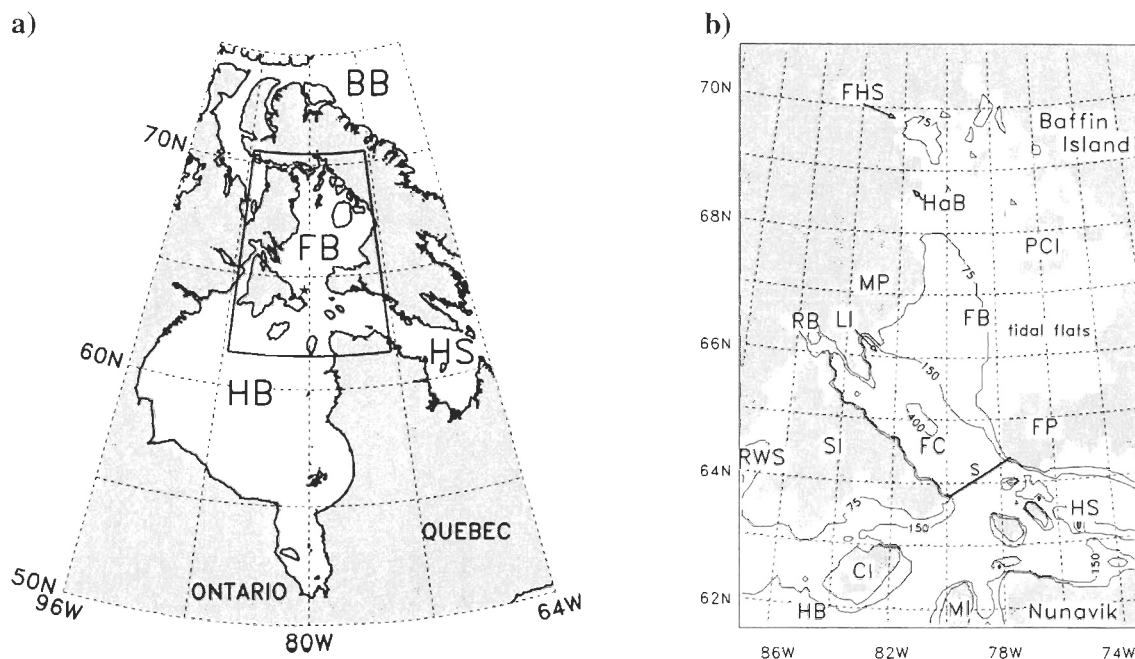


Fig. IV.1. Hudson Bay system (a) and Foixe Basin (b). In **a**, the star indicates the location of the mooring in Foixe Channel and the inset corresponds to Foixe Basin and its immediate surrounding neighbours, also shown in **b**. The model grid (partial, corresponding to the outputted data) is shown in **b** where the cross section S is symbolized by the straight bold line. The acronyms definitions are as follow: Baffin Bay (BB), Coats Island (CI), Foxe Basin (FB), Foixe Channel (FC), Fury and Hecla Strait (FHS), Foixe Peninsula (FP), Hall Beach (HaB), Hudson Bay (HB), Hudson Strait (HS), Lyon Inlet (LI), Melville Peninsula (MP), Mansel Islands (NI), Prince Charles Island (PCI), Repulse Bay (RB), Roes Welcome Sound (RWS) and Southampton Island (SI).

combined with the net freshwater input in the whole HB system. In other words, although there is 20 times less seawater passing through the HB system than through Davis Strait (0.1 Sv vs. 2 Sv), the difference reduces to around 3 times ($29 \times 10^{-3} + 6 \times 10^{-3} = 35 \times 10^{-3} \text{ Sv}$ vs. $100 \times 10^{-3} + 19 \times 10^{-3} = 119 \times 10^{-3} \text{ Sv}$) in terms of freshwater.

In winter, FB is almost completely covered by at least three kinds of sea-ice: a) ice formed through thermodynamic growth (spread all over the center of the basin); b) brown ice rich in trapped sediment (over FB's eastern tidal flats); and c) ice formed through compaction of frazil ice (in western FB's polynyas located at: Hall Beach, along MP's eastern coast and at Lyon Inlet). There is, however, no multi-year ice as the basin is generally ice-free by the end of summer. The mean river runoff in the basin is estimated at $620 \text{ m}^3\text{s}^{-1}$ (Hydat database, Department of Environment Canada). In addition, a strong gravity current originating from western FB's polynyas and characterized by the pulse-like propagation of around $1.5 \times 10^{12} \text{ m}^3$ of dense waters flowing at a mean speed of 2 cms^{-1} (Defossez *et al.*, 2008a) dramatically alters the deep circulation and the water column structure.

In summer, FB's circulation is of classical estuarine type characterized by strong tides, with the amplitude of the semi-diurnal constituent M2 reaching 2.4 m in eastern FB, and by significant freshwater input both from river, with a mean runoff up to $7600 \text{ m}^3\text{s}^{-1}$, and from oceanic freshwater flowing through FHS. This freshwater enters FB mainly at the north and subsequently flows southwards by following the cyclonic circulation that prevails in the basin. Since this incoming water is lighter than FB's seawater, it tends to flow at the surface (Prinsenbergh, 1986a) and the greater horizontal buoyancy gradient in summer is

likely to amplify the circulation. Also, the mean difference between precipitation (P) and evaporation (E) summed over the whole basin is $P - E = 2310 \text{ m}^3\text{s}^{-1}$, while it is only $-342 \text{ m}^3\text{s}^{-1}$ in winter (values obtained from the model of Saucier *et al.*, 2004, and averaged over the winter and summer periods defined in Section IV.3.1).

The ice cover is a distinctive and essential feature of polar seas as it alters dramatically the circulation pattern in winter by screening the winds and by adding friction and damping at the sea surface. In fact, it is so distinctive that it could almost be argued that comparing the winter and summer circulation in FB, the purpose of this study, does not make much sense since this is tantamount to comparing two quite different systems. However, the intrinsic inertia of the basin results in each season influencing the following, through preconditioning of water masses and/or delayed system response. For example: a) the higher freshwater input in summer enhances the stratification which certainly has an impact on the ice growth during the following winter; and b) some of the ice formed in FB is eventually exported to the LS, long after the winter has ended in the basin. The external influence of the other parts of the HB system can also play a role in the regulation of FB's estuarine circulation.

The distinction between an estuarine system, *i.e.* a system where the dominant pattern of the circulation is of estuarine type, and a true estuary is made in this study. This is important because all estuary definitions imply that these water bodies are connected with the open sea, the latter playing effectively the role of a water, salt, heat and tidal energy reservoir. This is clearly not the case of the whole domain of FB, since it is only indirectly connected to the Arctic and the LS, nor of the system of its individual coastal

areas associated with its main body since the basin has a total volume of only $18 \times 10^{12} \text{ m}^3$ of water and its bulk characteristics vary seasonally. Besides, the prevailing northwestern winds affect greatly the surface circulation in FB as well as, indirectly, the deep circulation when they open western FB's polynyas in mid-winter, which leads to the production of a dense water pulse (Defossez *et al.*, 2008a, b). The wind induced currents play therefore a greater role in the basin than what is generally found in estuaries.

The sea-ice formation during winter in high latitude estuarine systems acts in a fashion similar to evaporation at lower latitudes as it removes freshwater and increases the salinity of the water column. When this exceeds the freshwater input from runoff near the shores, the estuarine circulation is said to be inverse or negative (El-Sabh *et al.*, 1997). So far, negative estuarine circulation has attracted little attention from oceanographers. This may change in the context of global warming because, in polar seas, a same system may be of positive (or classical) type during summer and of negative type during winter, thus forming a positive-negative estuarine couple likely to be sensitive to climate changes (MacDonald, 2000). For an estuary open to an ocean like, for example, the Mackenzie River and the Arctic, the negative circulation is restricted near the shore, but for an inland sea like FB, the whole basin may be regarded as a wide negative estuarine system (Prinsenbergh, 1986a).

Although the negative estuarine circulation in winter in FB has already been mentioned in the literature, it has never really been demonstrated nor studied. The aim of this study is therefore to determine whether FB's estuarine circulation forms a positive-negative couple. This is mainly achieved by giving a detailed account, in winter and in

summer, of the seawater transport and salt balance between the basin and its surroundings parts. Most calculations in this paper are done with data obtained from the numerical model developed by Saucier *et al.* (2004a), except the tidal analysis which uses year-long time series of currents from a mooring in Foxe Channel (FC). The simulated and observed data are described in Section IV.2. The seasonal features of the circulation are detailed in Section IV.3 and the mass transfers between the surrounding parts of FB are quantified in Section IV.4. The effect of the sea-ice cover on the tidal circulation at mid-depth is analysed in Section IV.5. Finally, these results are discussed in Section IV.6, along with the conclusion.

IV.2. MODEL DESCRIPTION AND OBSERVATIONS

IV.2.1. Model

The numerical model developed and described in detail by Saucier *et al.* (2004a) is based on the GF8 model of Stronach *et al.* (1993); it has been adapted and validated to the HB system. It is a z-level, hydrostatic, shallow water and incompressible formulation, with atmospheric (air temperature, winds, cloud cover and precipitation) and runoff (momentum, temperature and salinity) forcings. The water levels are specified along the open boundaries and the initial conditions come from composite sets of observed and simulated data. Furthermore, the model is coupled to a dynamic and thermodynamic sea-ice and snow cover model. Although the numerical grid covers the whole system, only the data corresponding to FB are used in this study. These output data are the seawater and sea-ice currents, the seawater temperature and salinity, the sea-ice growth rate and thickness. Several other physical quantities, like the surface heat fluxes with the atmosphere, are also computed and used internally by the model, but are not exploited here. The grid's horizontal resolution is 10×10 km and its vertical resolution varies from 10 m at the surface to 30 m at the bottom of FC. The internal time step of the model is five minutes and the simulated data are averaged over a three hour period. In order to estimate how appropriate these spatial and time resolutions are, it is useful to calculate the internal Rossby radius which gives the scale of the baroclinic instabilities. For an idealized two layer ocean, this radius is:

$$r = \frac{1}{f} \sqrt{g \frac{(\rho_2 - \rho_1)}{\rho_1} \times \frac{h_1 h_2}{(h_1 + h_2)}} \quad (1)$$

where f is the Coriolis parameter, g is the gravitational acceleration, $\rho_{1,2}$ and $h_{1,2}$ are the upper (1) or lower (2) layer densities and depth, respectively. In the middle of FC, $f = 1.32 \times 10^{-4} \text{ s}^{-1}$, $\rho_1 = 1026.15 \text{ kg m}^{-3}$, $\rho_2 = 1027.93 \text{ kg m}^{-3}$, $h_1 = 75 \text{ m}$ and $h_2 = 450 \text{ m}$ (these values have been calculated with the model), which leads to $r \approx 8 \text{ km}$. In the middle of FB, $f = 1.34 \times 10^{-4} \text{ s}^{-1}$, $\rho_1 = 1026.55 \text{ kg m}^{-3}$, $\rho_2 = 1027.09 \text{ kg m}^{-3}$, $h_1 = 75 \text{ m}$ and $h_2 = 125 \text{ m}$, which leads to $r \approx 4 \text{ km}$. Since the grid cells are larger than r in both cases, the model can not resolve properly the small scale processes that may occur in FB and these latter must be parameterized if they are to be taken into account. However, only synoptic and mesoscale phenomena are studied here and the grid's resolution is therefore more than sufficient to allow accurate calculation of water, salt and ice transport.

One section (S) has been defined for the calculation of the transported physical quantities inside and outside FB; its location is shown in Fig. IV.1b. The section is comprised between the easternmost tip of SI and southwestern Foxe Peninsula (FP), *i.e.*, close to FB's outlet. S is a cross-section of FC, almost perpendicular to the channel's longitudinal axis; it is 114 km wide and the maximum depth along its length is 265 m.

In addition, Lagrangian tracers using the sea-ice velocity field in FB are used in order to determine ice floe trajectories from the start of three significant periods: a) when the sea-ice begins to form (in early November); b) at the climax of the sea-ice production rate (in early February); and c) when the sea-ice starts to melt (in early May). Note that the tracers exist as long as there is ice at the sea surface, independently of the ice thickness. In

addition, the procedure used here has been simplified by not dealing with ice floes running aground, in which case, the corresponding tracer is just terminated. The Lagrangian tracers are useful as they provide a time dependent picture of the sea-ice motion whereas the sole calculation of ice transport through a section gives no information about the fate of the ice outside FB.

IV.2.2. Observations

The current meter used for the tidal analysis is a S4 from InterOcean Systems Inc. It was deployed at a depth of 150 m from August 2004 to August 2005 and its location in FC was 64.37 °N and 80.55 °W (Fig. IV.1). At this location, which is close to S (113 km from the middle of the section), the depth of the channel is 360 m. The sampling rate of the horizontal current velocities u (eastward component) and v (northward component) was set to one hour with a precision of $\pm 3 \times 10^{-2} \text{ ms}^{-1}$. This mooring was part of the program MERICA (*MERs Intérieures du Canada*, Saucier *et al.*, 2004b), northern component, funded by the Department of Fisheries and Oceans, Canada.

It must be noted that the dense water mass mentioned in Section IV.1 and flowing at depth as a gravity current in the channel has a maximum thickness of 140 m. Therefore, the current meter was approximately 70 m ($= 360 - 150 - 140$) above the top of this incoming water mass and the record of the horizontal velocity is likely to be little affected by it. Furthermore, the depth of 150 m corresponds more or less to the topographic break distinguishing FC from the wide northern and shallow part of FB and therefore the horizontal velocity signal should not be affected by shallow water tidal constituents either.

The tidal analysis is based on the T_TIDE package developed by Pawlowicz *et al.* (2002) and the calculations are made under Matlab 7 (The MathWorks, Inc.). The current velocity has been decomposed between an axial component ($U_{//}$) and a transverse component (U_{\perp}), taking the length of FC and its perpendicular as reference axes (they correspond exactly to a 45° clockwise rotation of the orthogonal West-East South-North referential); the phase has been similarly decomposed ($\Phi_{//}$ and Φ_{\perp}). The five main tidal constituents considered in this study, which contain most of the tidal energy, are M2 (lunar semidiurnal, 12.42 hours), S2 (solar semidiurnal, 12.00 hours), N2 (lunar elliptic semidiurnal, 12.66 hours), K1 (luni-solar declinational diurnal, 23.93 hours) and O1 (lunar declinational diurnal, 25.82 hours).

IV.3. FOXE BASIN PHYSICAL OCEANOGRAPHY

IV.3.1. Winter and summer definition

The oceanographic climate in FB can conveniently be defined by means of the ice growth rate: a prolonged positive period corresponding to the winter and, inversely, a prolonged negative period corresponding to the summer. In Fig. IV.2, the simulated ice growth rate averaged over the whole domain of the basin shows that the year 2003-2004 can be split in two: the winter from October 22, 2003 to May 05, 2004 and the summer from May 05, 2004 to October 07, 2004. In this study, these two periods define the two seasons in the basin for all calculations made with the simulated data; the calculations include: 1) seawater, salt and sea-ice transport; 2) seawater temperature, salinity and velocity fields; 3) sea-ice growth rate, thickness and velocity fields; and 4) reconstruction of sea-ice trajectories with Lagrangian tracers. It is important to note that when the data are averaged over the whole winter or summer, each lasting about six months, the high frequency (like the tides) or short lived (like the dense water pulse at the bottom of FC) seasonal phenomena are smoothed out. Note also that the averages may introduce apparent phase shifts as water masses formed during one season are included in the calculations of the following one, but at different depths and/or locations.

IV.3.2. Sea-ice dynamics

The ice circulation in FB affects the general circulation by adding an actual physical

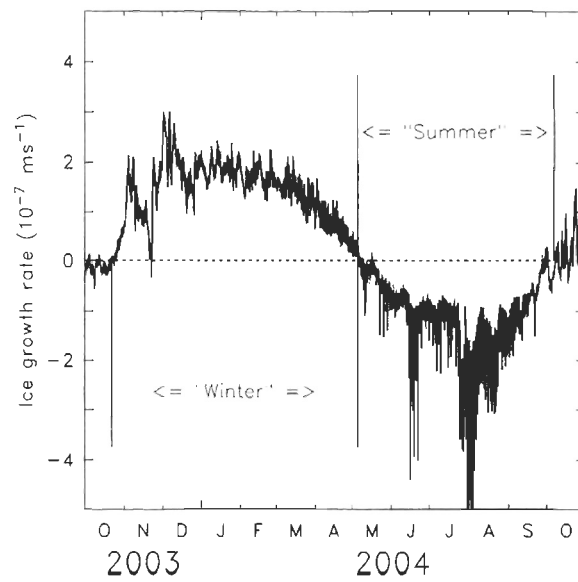


Fig. IV.2. Simulated ice growth rate averaged over Foxe Basin. The positive (negative) values correspond to the formation (melting) of sea-ice.

screen between the sea surface and the atmosphere and by quickly exporting large amounts of (frozen) freshwater. The time averaged sea-ice thermodynamic growth and velocity as well as the trajectory (Lagrangian tracers) of ice floes are detailed here in order to describe the ice dynamics in the basin. The growth and velocity fields are useful to give mesoscale information about the ice cover while the tracers are better suited to show where the ice floes are leaving FB. Some of the following results have already been discussed by Saucier *et al.* (2004a), but at the scale of the whole HB system.

In Fig. IV.3, the ice growth field in FB clearly features three distinct areas: a) a high production rate zone of sea-ice along the eastern coast of MP, with values exceeding $3.5 \times 10^{-7} \text{ ms}^{-1}$, corresponding to FB's latent heat coastal polynyas; b) a large central zone with production rates of about $1.5 \times 10^{-7} \text{ ms}^{-1}$; and c) a small zone around FP's southwestern coast with high negative production rates reaching $-6 \times 10^{-7} \text{ ms}^{-1}$. The first area has already been extensively described by Defossez *et al.* (2008a, b) who found that high heat losses over the polynyas lead to the formation of large amount of frazil ice. The third area strongly suggests that there is upwelling providing sensible heat underneath the pack ice. The ice velocity field presents a very distinctive "rack and pinion" pattern in FB: a significant ice current flows southward at the west of the basin while a gyre around 180 km in diameter covers a large portion of the eastern part. The relatively high values of the ice velocity field in FB ($0.25 \pm 0.09 \text{ ms}^{-1}$, averaged over the whole basin) contrasts with the weak ice current seen in northern HB ($0.11 \pm 0.09 \text{ ms}^{-1}$, averaged over the northern part of the bay). Fig. IV.3 shows also that there is a continuity between FB's and HS's ice currents, suggesting that most of the sea-ice exported by the basin enters subsequently the strait.

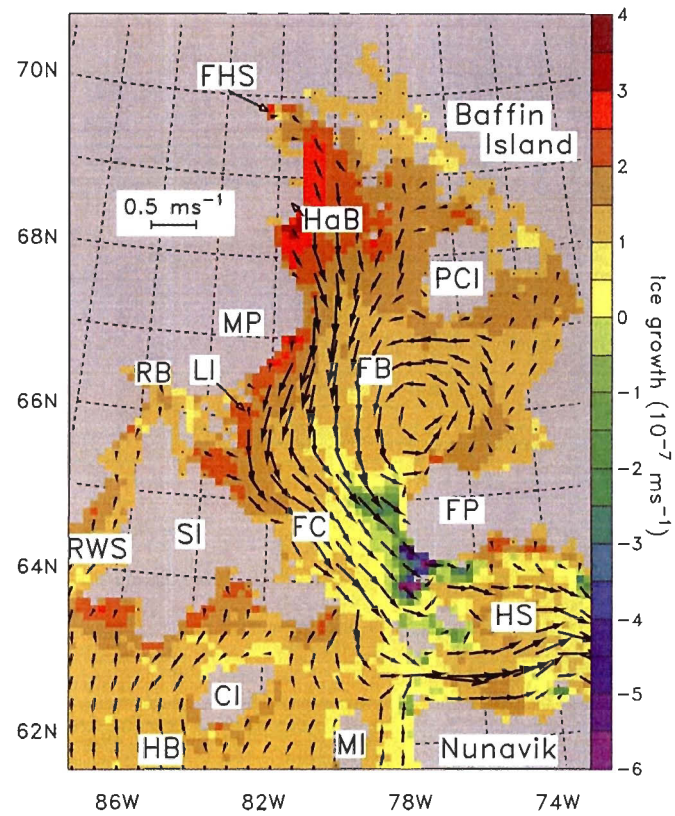


Fig. IV.3. Simulated ice growth rate averaged over the winter in Foxe Basin. The positive (negative) values correspond to the formation (melting) of sea-ice. The vector field corresponds to the sea-ice velocity, its scale is given in the upper left box. (see Fig. IV.1 for acronym definitions)

Since the section S corresponds to the main fairway between the basin and the other parts of the HB system, ten tracers ($T_{1 \text{ to } 10}$) have been spread evenly along its width in order to determine the fate of the sea-ice leaving FB. Their trajectories are shown in Fig. IV.4; in addition, the mean speed and total distance covered by each tracer is reported in Table IV.1.

At the beginning of the ice formation (Fig. IV.4a), the majority of the tracers flows toward HS although their trajectory is somehow erratic. The complex made of the three small islands at the head of HS clearly separates the ice flow into a direct route south of FP and a longer one bypassing the islands by the south. The speed of the tracers entering HS by taking the longest route (*e.g.*: $\sim 0.3 \text{ ms}^{-1}$ for $T_{4 \text{ and } 5}$) is a bit faster than the others (*e.g.*: 0.19 ms^{-1} for T_{10}); this may be due to the efficient surface currents in the strait, the latter being sparsely covered by sea-ice during this time.

The situation changes appreciably during the maximum ice formation (Fig. IV.4b): all tracers enter HS and their trajectories are smoother. Furthermore, their speed seems to be greater as they were close to FP at the start of the run (from 0.16 ms^{-1} for T_2 to 0.27 ms^{-1} for T_8) suggesting that the surface currents in the strait have now been reduced by the friction with the sea-ice.

The situation is even more different at the beginning of the melting of ice (Fig. IV.4c): all tracers penetrate deeply into northeastern HB, without however flowing much below the 62°N parallel at which point they perform a "U-turn" toward HS. It is possible that this ice is driven by the strong coastal current, which has been described by Saucier *et al.* (2004), flowing along eastern HB toward HS. Here also, the speed of the tracers seems greater as they were close to FP at the start of the run (from 0.13 ms^{-1} for T_2

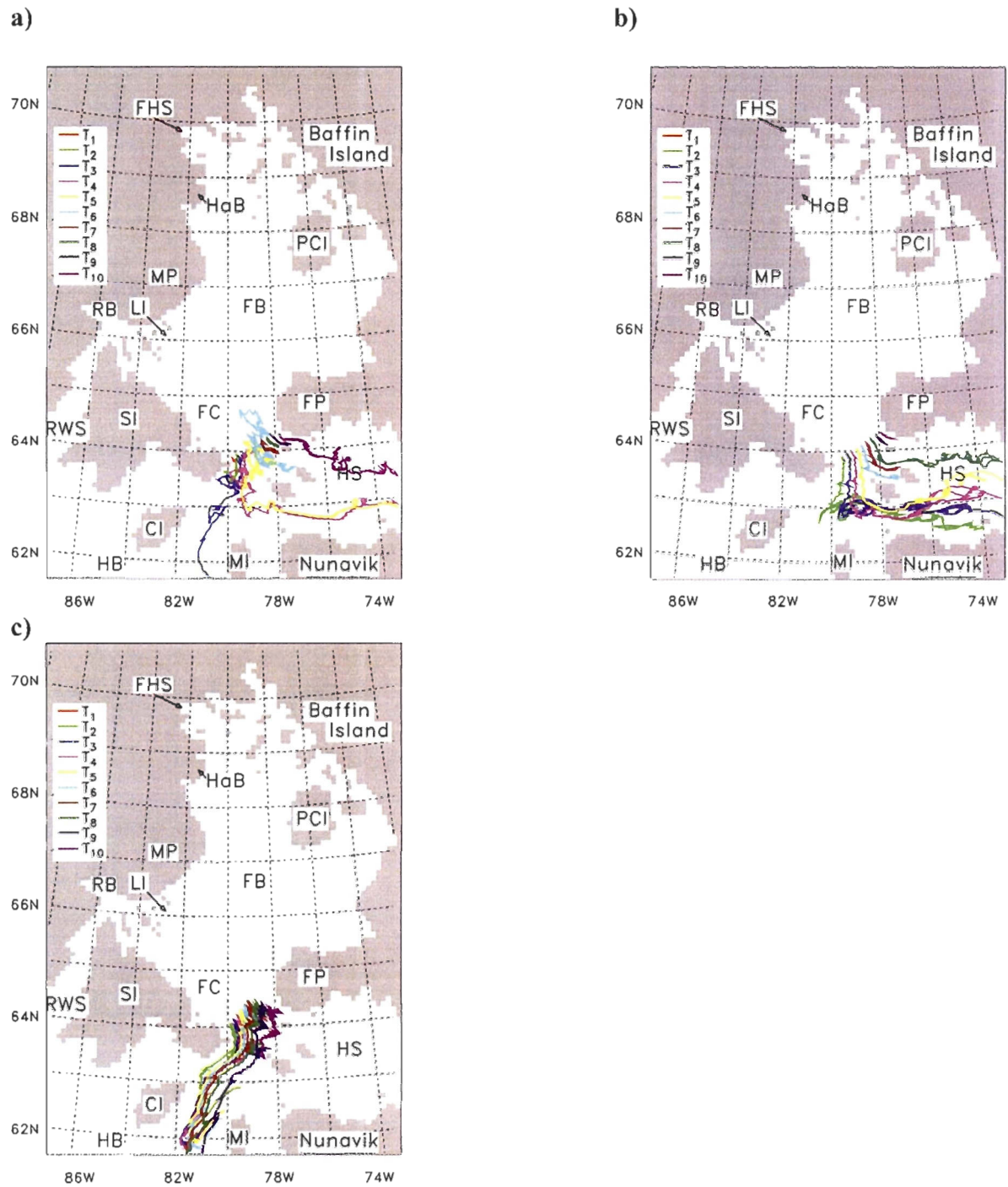


Fig. IV.4. Simulated sea-ice trajectory in Foxe Basin. The color code of the tracers corresponding to the trajectories is given in the upper left box. In **a**, **b** and **c** the run starts in November 1, 2003, February 1, 2004 and May 1, 2004, respectively. (see Fig. IV.1 for acronym definitions)

	T ₁	T ₂	T ₃	T ₄	T ₅	T ₆	T ₇	T ₈	T ₉	T ₁₀
11-01-03	0.18 17	0.14 233	0.19 837	0.26 1135	0.32 1465	0.40 1601	0.29 180	0.15 79	0.11 95	0.19 935
02-01-04	0.01 0	0.16 2428	0.19 2586	0.21 1353	0.23 1218	0.11 389	0.20 320	0.27 1404	0.16 89	0.13 87
05-01-04	0.02 0	0.13 994	0.15 1168	0.16 1237	0.17 1283	0.18 1367	0.19 1340	0.20 1379	0.21 1349	0.25 759

Table IV.1. Mean speed and total distance covered by the Lagrangian tracers leaving Foxe Basin (see Fig. IV.4 for trajectories). The dates indicate the start of each run (beginning of ice formation, maximum of ice formation and beginning of ice melting). The speed (top of each cell) is in ms^{-1} and the distance (bottom of each cell) is in km.

to 0.25 ms^{-1} for T_{10}). Note that their trajectory ends because their supporting ice has melted and that the melted ice seems to flow toward HS. This indicates that even if some ice or melted ice coming from FB enters HB, it is likely to leave the bay and enter HS. In other words, northeastern HB is only a stage travel and all exported FB's sea-ice eventually flows into HS.

IV.3.3. Water characteristics and mean circulation

Saucier *et al.* (2004a) confirmed that the mean circulation in FB is cyclonic in all seasons, but Fig. IV.1b clearly indicates that the northern part of the basin is less than 150 m deep while the southern part, *i.e.* FC, reaches 450 m depth; this implies that a large volume of surface water cyclically flows over small and great depths. Roughly, a parcel of water at 150 km from the center of the cyclonic loop, which is close to FB's center, makes 73 days to complete a turn if the mean annual current is around 0.15 ms^{-1} for the layer between the surface and 60 m depth (value obtained with the numerical model). Since the basin is well delimited by land and islands, there is a relative continuity in FB's surface water characteristics, but, because of the topography, not in its circulation. The problem becomes even more complex when considering the deep waters in FC which have a quite different oceanographic cycle. Studying FB's circulation requires therefore to chose between an approach favoring the description of the currents, which implies to describe the shallow and deep parts of the basin separately, or an approach favoring the water characteristics, which implies the description of the basin as a whole. Since the deep circulation in FC strongly depends on surface phenomena (Defossez *et al.*, 2008a, b), the

second approach has been preferred here. The seawater characteristics and circulation are therefore examined in this section both at the surface (first layer of the numerical grid: thickness = 10 m and depth = $10/2 = 5$ m) and near the bottom (last layer of the numerical grid: thickness and depth depending on the bathymetry, so that the layer is at most 30 m thick and the depth is, in average, $20 + 30/2 = 35$ m above the bottom in the deepest parts and much less in the shallower parts) of the basin. This is tantamount to considering only the lighter and denser water masses in the basin but gives an interesting insight into the exchanges between the different parts of the HB system. The bulk circulation is implicitly treated in Section IV.4 with the calculation of mass transports. Here, the simulated temperature and salinity distributions are described at the scale of the basin. Furthermore, the surface velocity fields have been plotted over each figure in order to visualize the main circulation in FB.

IV.3.3.1. In winter

IV.3.3.1.1. At the surface

The surface velocity field (Fig. IV.5a or b) shows a globally cyclonic circulation in FB. The mean winter value of the surface current averaged over the whole domain of FB is $0.35 \pm 0.09 \text{ ms}^{-1}$. It can be seen at the level of the section S that the current tends to flow outside the basin.

The sea surface temperature (SST, Fig. IV.5a) is close to the freezing point ($-1.85 \text{ }^\circ\text{C}$) over almost all the domain of FB because of air temperatures commonly below